

ORNL/TM-10759

**OAK RIDGE
NATIONAL
LABORATORY**

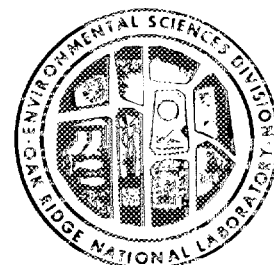
MARTIN MARIETTA

**Characterization of Clay Minerals
and Organic Matter in Shales:
Application to High-Level
Nuclear Waste Isolation**

N. Güven
C. R. Landis
G. K. Jacobs

Environmental Sciences Division
Publication No. 3136

OAK RIDGE NATIONAL LABORATORY
CENTRAL RESEARCH LIBRARY
CIRCULATION SECTION
4500N ROOM 111
LIBRARY LOAN COPY
DO NOT TRANSFER TO ANOTHER PERSON
If you wish someone else to see this
report, send in name with report and
the library will arrange a loan.



OPERATED BY
MARTIN MARIETTA ENERGY SYSTEMS, INC.
FOR THE UNITED STATES
DEPARTMENT OF ENERGY

Printed in the United States of America. Available from
National Technical Information Service
U.S. Department of Commerce
5285 Port Royal Road, Springfield, Virginia 22161
NTIS price codes—Printed Copy: A05 Microfiche A01

This report was prepared as an account of work sponsored by an agency of the United States Government. Neither the United States Government nor any agency thereof, nor any of their employees, makes any warranty, express or implied, or assumes any legal liability or responsibility for the accuracy, completeness, or usefulness of any information, apparatus, product, or process disclosed, or represents that its use would not infringe privately owned rights. Reference herein to any specific commercial product, process, or service by trade name, trademark, manufacturer, or otherwise, does not necessarily constitute or imply its endorsement, recommendation, or favoring by the United States Government or any agency thereof. The views and opinions of authors expressed herein do not necessarily state or reflect those of the United States Government or any agency thereof.

ENVIRONMENTAL SCIENCES DIVISION

CHARACTERIZATION OF CLAY MINERALS AND ORGANIC MATTER IN SHALES:
APPLICATION TO HIGH-LEVEL NUCLEAR WASTE ISOLATION

N. Güven*, C. R. Landis*, and G. K. Jacobs

Environmental Sciences Division
Publication No. 3136

*Department of Geosciences, Texas Tech University, Lubbock, Texas

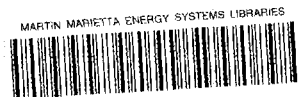
NUCLEAR AND CHEMICAL WASTE PROGRAMS

Date Published-- October 1988

Notice: This document contains information of a preliminary nature.
It is subject to revision or correction and therefore does
not represent a final report.

Prepared for the
Office of Civilian Radioactive Waste Management
(Activity No. DB 02 04 02 0)

Prepared by the
OAK RIDGE NATIONAL LABORATORY
Oak Ridge, Tennessee 37831
operated by
MARTIN MARIETTA ENERGY SYSTEMS, INC.
for the
U.S. DEPARTMENT OF ENERGY
under contract DE-AC05-84OR21400



3 4456 0282993 7

CONTENTS

	<u>Page</u>
LIST OF FIGURES	v
LIST OF TABLES	ix
ABSTRACT	xi
EXECUTIVE SUMMARY	xiii
1. INTRODUCTION	1
2. MATERIALS	6
3. ANALYSIS OF MINERAL MATTER BY X-RAY DIFFRACTION AND ELECTRON MICROSCOPY	7
3.1 METHODS	7
3.1.1 X-ray Diffraction	7
3.1.2 Electron Microscopy	7
3.2 RESULTS	8
3.2.1 Chattanooga Shale	8
3.2.2 Alum Shale	18
3.2.3 Green River Formation	23
3.3 DISCUSSION	25
4. ANALYSIS OF ORGANIC MATTER IN SHALES BY FLUORESCENCE MICROSCOPY	26
4.1 METHODS	27
4.2 RESULTS	29
4.2.1 Macerals	29
4.2.2 Vitrinite Reflectance Analysis	33
4.2.3 Quantitative Fluorescence Analysis	38
4.2.4 Temporal Fluorescence Analysis	41
4.3 DISCUSSION	41
5. TIME-RESOLVED FLUORESCENCE SPECTRA OF STANDARD ORGANIC COMPOUNDS	46
5.1 METHODS	47
5.2 RESULTS	50
5.3 DISCUSSION	53
6. REFERENCES	58

LIST OF FIGURES

<u>Figure</u>		<u>Page</u>
3.1	Chattanooga Shale; 44,000X; untreated	10
3.2	Chattanooga Shale; 135,000X; untreated	10
3.3	Chattanooga Shale; 65,000X; untreated	11
3.4	Chattanooga Shale; 45,000X; untreated	11
3.5	Chattanooga Shale; untreated	12
3.6	Chattanooga Shale; 30,000X; untreated	12
3.7	Chattanooga Shale; 65,000X; 100°C heat treatment	15
3.8	Chattanooga Shale; 65,000X; 300°C heat treatment	15
3.9	Chattanooga Shale; 135,000X; 300°C heat treatment	16
3.10	Chattanooga Shale; 45,000X; 400°C heat treatment	16
3.11	Chattanooga Shale; 35,000X, 400°C heat treatment	17
3.12	Chattanooga Shale; 45,000X; 500°C heat treatment	17
3.13	Chattanooga Shale; 90,000X; 500°C heat treatment	19
3.14	Chattanooga Shale; 35,000X; 600°C heat treatment	19
3.15	Chattanooga Shale; 27,000X; 600°C heat treatment	20
3.16	Chattanooga Shale; 35,000X; 600°C heat treatment	20
3.17	Alum Shale; 27,000X; untreated	21
3.18	Alum Shale; 27,000X; untreated	21
3.19	Alum Shale; untreated	22
3.20	Alum Shale; 35,000X; 600°C heat treatment	24
3.21	Alum Shale; 27,000X; 600°C heat treatment	24

<u>Figure</u>	<u>Page</u>
4.1 Photomicrograph of Alum Shale vitrinite like organic material in a mineral matrix including conspicuously bright pyrite (reflected white light at 750X)	31
4.2 Photomicrograph of Green River Formation vitrinite (reflected white light at 750X)	31
4.3 Photomicrograph of Chattanooga Shale vitrinite in mineral groundmass (reflected white light at 750X)	32
4.4 Photomicrograph of untreated Chattanooga Shale alginite	32
4.5 Photomicrograph of positive alteration of Alum Shale liptinite	34
4.6 Photomicrograph of organic-rich laminae of the Green River Formation	34
4.7 Variation of mean random vitrinite like (Alum Shale) and vitrinite (Green River Formation and Chattanooga Shale) reflectance as a function of increasing temperature of heat treatment	37
4.8 Photomicrograph of yellow-orange alginite in Chattanooga Shale heat treated to 300°C (reflected blue light at 750X)	39
4.9 Fluorescence spectra of untreated and heat-treated (300°C) alginite from the Chattanooga Shale showing the shift to longer wavelengths as a function of thermal treatment	40
4.10 Fluorescence lifetime distributions of Chattanooga Shale as a function of thermal treatment	42
4.11 Fluorescence lifetime distribution of untreated Alum Shale alginite clearly showing the high percentage of the subnanosecond component	43
5.1 Schematic diagram of laser fluorescence system showing the input Hg bulb (left) and nitrogen-pumped, tunable-dye laser (right)	48
5.2 Graphical output of spectral (top) and temporal (bottom) fluorescence analyses	54

<u>Figure</u>		<u>Page</u>
5.3	Spectral shift of linearly fused aromatics	55
5.4	Time-resolved data of fluorescence decay times and emission intensity over the spectral range of 390 to 470 nm for anthracene, POPOP, and a mixture of the two (Borst et al., 1987)	56

LIST OF TABLES

<u>Table</u>	<u>Page</u>
3.1 Interplanar spacing of the 001-reflection of illite as a function of heat treatment for 24 h	9
3.2 X-ray spectral intensity data on Chattanooga Shale (intensity ratios relative to the K line of silicon) . . .	14
3.3 Elemental ratios (relative to Si) in illite particles as obtained from X-ray spectra in Table 3.2	14
3.4 X-ray spectral intensity data on Alum Shale (intensity ratios relative to the K line of silicon)	22
3.5 Elemental ratios (relative to Si) in the illite particles in Table 3.4	23
4.1 Pairs of white- and blue-light maceral analyses of Chattanooga, Alum, and Green River Formation shales showing their compositional diversity and improved detection of liptinites in blue-light	30
4.2 Mean random vitrinite reflectances for shales that did not combust during heat treatment	36
4.3 Average fluorescence parameters for the Chattanooga Shale (alginite), Green River Formation (fluorescent fillings), and the Alum Shale (alginite)	39
5.1 Listing of absorbances of the compounds included in this study	51
5.2 Spectral and temporal properties of the fluorescing compounds	52

ABSTRACT

Güven, N., C. R. Landis, and G. K. Jacobs. 1988.
Characterization of clay minerals and organic matter in
shales: Application to high-level nuclear waste
isolation. ORNL/TM-10759. Oak Ridge National
Laboratory, Oak Ridge, Tennessee. 82 pp.

The objective of the Sedimentary Rock Program at the Oak Ridge National Laboratory is to conduct investigations to assess the potential for shale to serve as a host medium for the isolation of high-level nuclear wastes. The emphasis on shale is a result of screening major sedimentary rock types (shale, sandstone, carbonate, anhydrite, and chalk) for a variety of attributes that affect the performance of repositories. The retardation of radionuclides was recognized as one of the potentially favorable features of shale. Because shale contains both clay minerals and organic matter, phases that may provide significant sorption of radioelements, the characterization of these phases is essential. In addition, the organic matter in shale has been identified as a critical area for study because of its potential to play either a favorable (reductant) or deleterious (organic ligands) role in the performance of a repository sited in shale.

Three shales, the Chattanooga Shale, the Alum Shale, and the Green River Formation were investigated in this three-part study. In the first part, the clay mineralogy of these shales was characterized as a function of 24-h heat treatments from ambient to 600°C. No significant changes occurred, except the oxidation of pyrite to hematite. In both untreated and heat-treated specimens, iron oxide coatings tend to cover the surfaces of the illite particles, thus potentially affecting the sorption properties of these clay minerals. In the second part of the study, spectral and temporal fluorescence microscopy was used to characterize the maceral compositions of these shales. It was found that a combination of white- and blue-light analyses allowed the most complete description of the maceral compositions. Shifts to longer wavelengths and increased percentages of subnanosecond lifetimes in the

wavelengths and increased percentages of subnanosecond lifetimes in the fluorescence of the macerals could be followed as a function of the heat treatments. Analyses of standard organic compounds, the third part of the study, were undertaken to evaluate the potential of using the quantification of microfluorometry to characterize the organic matter dispersed in sedimentary rocks. It was found that systematic relationships existed for both spectral and temporal fluorescence data and that mixtures of organic compounds could be identified with this technique.

EXECUTIVE SUMMARY

A combination of X-ray diffraction and electron microscopy was used to characterize the mineralogic constituents of the Chattanooga Shale, Alum Shale, and Green River Formation both before and after heat treatments. The mineralogic compositions of these samples are reasonably consistent with results from Lee, Hyder, and Alley (1988). Heat treatments (24 h) up to 600°C result in few mineralogic changes, with the exception of the oxidation of pyrite to hematite. Illite, the predominant clay mineral in these shales, was found to be similar to the standard Silver Hill illite and did not undergo significant alteration during the heat treatments. Iron oxides typically occurred as coatings on the surface of the illites, an important consideration when interpreting results from sorption experiments because the oxide coatings may interfere with ion-exchange reactions of radionuclides. The coatings themselves may also act as strong adsorbents for some radionuclides under certain geochemical conditions (e.g., basic pH conditions); therefore, further detailed study using these microanalytical techniques combined with autoradiography could yield some useful results.

The fluorescence properties of whole-rock mounts of thermally altered Alum Shale, Chattanooga Shale, and Green River Formation shale were studied petrographically using white- and blue-light techniques. Each of these shales possesses a unique maceral assemblage that is better studied using a combined maceral analysis. More liptinites are counted in blue light, where the contrast between the maceral and the mineral matrix is greatest. For example, liptinites in laminae from the Green River Formation are easily revealed by their fluorescence properties. Similarly, the strong yellow fluorescence of the alginites of the Chattanooga Shale contrasts sharply with the largely nonfluorescent mineral matrix. Changes as a function of thermal treatment can also be monitored petrographically. Vitrinite reflectance varies systematically and uniquely for these shales. These early results indicate that vitrinite reflectance may be used as a

thermometer of rapid thermal alteration (much like it is used for coals and petroleum source rocks). In this case, the Chattanooga and Green River Formation shales follow similar maturation paths despite their age and compositional differences. Alginite spectra also vary systematically with increasing temperature, recording a shift to the longer wavelengths from the yellow to the orange (561 to 626 nm). The shift to the orange wavelengths at 300°C correlates well with a broad exothermic Differential Thermal Analysis (DTA) peak that occurs from roughly 340 to 480°C. Temporal analyses indicate fluorescence lifetime distributions heavily favoring subnanosecond components, particularly as temperature and rank increase. For the Chattanooga Shale alginites, nanosecond and subnanosecond fluorescence lifetimes are recovered at low thermal treatment temperatures. However, as the temperature of the heat treatment increases, the distribution clearly favors the shorter, subnanosecond lifetimes. The techniques employed in this portion of the study demonstrate the potential utility of microfluorometry in describing the behavior of organic matter in shales under a variety of conditions. It would be especially interesting to combine these techniques with autoradiography to investigate which organic phases may be most reactive to radioelements. The alteration of kerogen during hydrothermal reaction could also be characterized, allowing more insight into the degradation of kerogen and the formation of potential organic complexants. Further quantification and refinement of these techniques will be necessary to advance studies such as these.

The fluorescence properties of a group of low-molecular-weight organic compounds were analyzed using a Leitz MPV III Orthoplan microscope interfaced on the input end with a 100-W Hg-arc lamp and nitrogen-pumped tunable-dye laser for both continuous-wave and pulsed-laser near-uv (365 and 395 nm, respectively) excitation. Resultant data extracted from the emission spectra are the spectral maximum and quotient. Temporal data from the analyzed decay curves include percentage contributions, fluorescence lifetimes (nanosecond and subnanosecond), and Einstein A-coefficients (intensity coefficients). These temporal data are acquired from iterative reconvolution or

recovered as a distribution of user-defined lifetimes. In either case, characteristic lifetimes for each fluorescing compound are recovered. The group of organic compounds studied included the alkanes, alkenes, alkynes, carboxylic acids, heteroatoms, and several linearly fused aromatics. Alkanes do not fluoresce and most of the other compounds that contain π -bonds were also observed not to fluoresce. Indeed, they did not absorb uv light (333 nm). Nonaromatic compounds fluoresce strongest in the blue wavelengths. Linearly fused aromatics display a shift to the longer wavelengths and decrease in fluorescence intensity as each additional ring is added to the structure. The fluorescence lifetimes of these compounds are predominantly in the nanosecond range, with subnanosecond lifetimes contributing less to the total emission. Thus, despite current limitations, time-resolved fluorescence microscopy is a viable technique worthy of continued developmental research. The identification and estimation of specific organic compounds in sedimentary rocks would be a significant advancement. To accomplish this advancement, further research is needed in (1) the analysis of additional individual compounds that may be common to organic matter in sedimentary rocks, (2) the investigation of dilution effects on the fluorescence characteristics, (3) the properties of organic compound mixtures, and (4) the characterization of fluorescence spectra of organic compounds in a variety of mineral matrices.

1. INTRODUCTION

The objective of the Sedimentary Rock Program (SERP) at the Oak Ridge National Laboratory is to conduct investigations to assess the potential for shale to serve as a host medium for the isolation of high-level radioactive wastes. The emphasis on shale is a result of screening major sedimentary rock types (shale, sandstone, carbonate, anhydrite, and chalk) for a variety of attributes that affect the performance of repositories. Results from studies using a ranking methodology that considered the technical aspects of geology, geochemistry, hydrology, thermal performance, rock mechanics, natural resources, waste package degradation, costs, and systems analyses suggested that shales offer the best potential for the safe isolation of wastes (Croff et al. 1986). The geologic characteristics of shales constitute a rather broad spectrum. Therefore, more detailed studies on the hydrologic, geochemical, and thermomechanical properties of various shales have been undertaken to identify relationships between the geologic characteristics of shales and the performance aspects of a repository. To address the variability among shales, end-member types were chosen for study within SERP. Lee, Hyder, and Alley (1988) discuss the four main types of shales that are being studied: organic-, smectite-, illite-, and carbonate-rich members.

The mineralogic characteristics of shales are important to the performance of a repository in several ways. For example, the chemistry of groundwaters in shales can be controlled at least partially by the mineralogy of the host formation (Von Damm 1987; Von Damm and Johnson 1987). These geochemical conditions are important to the stability of waste package materials (e.g., metallic containers, clay packings, and waste forms) that control the containment and release of waste elements. The migration of radionuclides through shale formations is also affected by mineralogic properties of the host rock. Specific phases may act as sorption sites for radionuclides migrating slowly through the rock. Reactions important to the retardation of radionuclides include ion exchange, precipitation,

adsorption, complexation, and oxidation-reduction. One of the main reasons for the favorable ranking of shales is the large apparent affinity of clay minerals, the predominant mineral phase in shales, for sorbing radioelements (see Table D.2.3 in Croff et al. 1986).

Many of the radioelements that are most important to the safety of a repository (e.g., U, Pu, Np, Tc) are sensitive to redox conditions. These elements are generally less soluble and more highly sorbed under reducing conditions. The organic matter in shales is typically thought to play a large role in the concentration of uranium (Bell 1978) and, by analogy, may be important in the retardation of other redox-sensitive elements. In addition to this potentially favorable aspect of acting as a reductant, organic matter in shale may act as a source for organic ligands that could increase the mobility of radioelements. For example, the reaction of kerogen in hydrothermal solutions at elevated temperatures has been shown to result in significant concentrations of aromatic and aliphatic hydrocarbons (Eglinton et al. 1986; Huizinga, Tannenbaum, and Kaplan 1987; Kawamura and Kaplan 1987). The presence of certain mineral phases during the hydrous pyrolysis experiments was found to influence the yield of some organic compounds. Fisher (1987) found acetate to be the predominant organic acid present in deep subsurface groundwaters. Thornton and Seyfried (1987) and Von Damm (1988) experimentally produced acetate and other organics during the hydrothermal reaction of sediment from the Guaymas Basin and seawater. Drummond and Palmer (1986) found acetate to be a strong complexant for iron at elevated temperatures and have suggested that it could also be a strong complex for uranium in carbonate-free waters under certain conditions. Even at the elevated temperatures expected near waste packages, the kinetics of acetate decomposition are slow enough that it could be an important complex to consider in modeling the performance of a repository (Palmer and Drummond 1986; Drummond and Palmer 1986). The evidence cited above suggests that it is important to assess whether the presence of organic matter, predominantly kerogen, in shales will be a deleterious or favorable condition for siting a repository.

Kerogen, the insoluble organic matter found in shales, is composed of various types of organic matter, called macerals, which can be thought of as the organic equivalent to minerals. Three maceral groups are generally recognized: (1) liptinites (derived from leaf cuticle, spores, pollen, plant waxes, fats, oils, and resins); (2) vitrinites (preserved woody tissue from plants); and (3) inertinite (woody material that has been altered through oxidation, mouldering, and biological attack). The chemical nature of the kerogen present in rocks is usually a function of both the source material and the diagenetic changes that have occurred since deposition. The importance of the potential interaction between the mineral matter and the kerogens in shales is indicated by the studies illustrating the role of minerals as catalysts for the production and decomposition of organic compounds in hydrothermal solutions (Palmer and Drummond 1986; Eglinton et al. 1987; and Huizinga, Tannenbaum, and Kaplan 1987).

The purpose of this study was to investigate a new technique for the elucidation of both the spatial distribution and chemical composition of organic matter in shales. Typically, the chemical composition of organic matter in shales has been determined using extraction and/or pyrolysis techniques coupled with gas chromatography/mass spectrometry, infrared spectroscopy, nuclear magnetic resonance, etc. These techniques, excellent for characterizing details of the organic structure in bulk samples, are not capable of providing information on the spatial distribution of organic matter, especially nondestructively. Lyons et al. (1987) have recently demonstrated the utility of a laser microprobe for the analysis of coal macerals.

Fluorescence techniques have been widely used to identify discrete organic matter in various source rocks and coals (Teichmüller 1986) and are excellent for identifying the general nature of macerals. Recent advances in spectral fluorescence analysis have allowed more quantitative interpretations of the nature of organic matter (Bertrand, Pitton, and Bernaud 1986; Khorasani 1987; and Martinez, Pradier, and Bertrand 1987). For example, the role of dilution and matrix effects

on fluorescence spectra have been investigated by Bertrand, Pitton, and Bernaud (1986). Khorasani (1987) has shown that fluorescence spectra can be used in combination with extraction methods to qualitatively measure the concentrations of saturates, highly alkylated aromatics, and condensed aromatics. Although significant accomplishments, these developments remain at the qualitative level.

The advent of temporal microfluorometry using pulsed-laser fluorescence has allowed more detailed interpretation of the nature of kerogens (Landis et al. 1987; James et al. 1987). Further refinement of this technique so that individual organic compounds could be identified within a rock specimen would allow a significant insight into actual geochemical processes. For example, it would be possible to (1) locate the presence of potential complex-forming organic molecules, (2) identify those organics most reactive to radionuclides by combining microfluorometry with autoradiography, (3) assess changes in the organic matter during water-rock interactions, and (4) evaluate the role of radiolysis on organic matter in shale specimens.

This three-part study was designed to address the potential for further quantification of microfluorometric analysis. The purpose of the first part of the study was to obtain fundamental information on the clay mineralogy of selected shale samples. The samples were analyzed both before and after heat treatments to help distinguish certain mineralogical characteristics and to provide preliminary information on the effects of heating on the shales. This information is important in evaluating the spatial relationships between clay minerals and the organic matter because, as discussed above, clay minerals can influence both the degradation rates and resulting products from organic-water interactions.

Part two of the study consisted of a fluorescence and vitrinite reflectance analysis of the samples to identify their maceral components and maturity. These studies provide basic data on the macerals present and confirm that the samples being studied are representative of the end-member shales. In addition, time-domain

analyses of these samples illustrate the ability of temporal analyses to identify mixtures of maceral fluorophores.

The third part of the study consisted of analyzing low-molecular-weight organic compounds using temporal fluorescence techniques to assess the potential for quantitatively identifying specific organic groups (e.g., carboxylic acids) that may be present in sedimentary rocks. The goal of this part of the study was to illustrate that individual organic compounds fluoresce with distinct characteristics that may be quantified with further study.

2. MATERIALS

Lee, Hyder, and Alley (1988) studied five shales representing end-member compositions: (1) Chattanooga Shale, (2) Pierre Shale, (3) Nolichucky Shale, (4) Pumpkin Valley Shale, and (5) Green River Formation. For this study, the organic-rich shales of the Green River Formation and the Chattanooga Shale were chosen because of their high organic content (11 and 13 wt %, respectively). In addition, the Alum Shale of Sweden was included because of its high organic carbon content, its highly uraniferous qualities (Bell 1978), and its potential to provide information on the processes important to the immobilization of uranium and, by analogy, other actinides.

The Chattanooga Shale sample is from the Upper Dowlletown Member of the formation in Fentress County, Tennessee. The sample is from a core and was taken from the depth interval 141 to 142 m. It is composed of illite (49 wt %), quartz/feldspar (25 wt %), organic matter (11 wt %), pyrite (6 wt %), chlorite/kaolinite (4 wt %), and other accessory minerals (Lee, Hyder, and Alley 1988). The shale is moderately dark gray and the organic matter tends to occur in micropores and as discontinuous laminae consisting of uniform mixtures of clays and organic matter.

The Green River Formation sample is from Garfield County, Colorado. The samples were obtained from drill cores into the roof of the Colony Mine. It is composed of carbonates (42 wt %), quartz/feldspar (28 wt %), organic matter (13 wt %), and illite (10 wt %). The sample is a laminated buff-to-medium brown shale, and the organic matter fills pores of irregular sizes and shapes (Lee, Hyder, and Alley 1988).

The Alum Shale sample is from the uranium-rich zone near Närke, Sweden. It is a late-Cambrian black shale, with typical organic carbon contents of 10 wt % but local occurrences of 20 to 30 wt % (Andersson et al. 1985). The sample is brownish-gray and quite fissile.

3. ANALYSIS OF MINERAL MATTER BY X-RAY DIFFRACTION AND ELECTRON MICROSCOPY

3.1 METHODS

Representative chips of the shale samples from the Chattanooga, Alum, and Green River Formations were finely ground to a uniform size (between 60 and 40 mesh). Portions of these powders were heated for 24 h over a temperature range of 100 to 600°C in 100°C increments at otherwise atmospheric conditions. Temperatures were monitored at least once per hour during the day and were maintained within 5°C of the target temperature. At 500 and 600°C all samples combusted readily, while the sample of Alum Shale combusted at 400°C.

3.1.1 X-ray Diffraction

The bulk powders were mixed with 10% LiF (for an internal standard), randomly packed into an aluminum holder, and x-rayed from $2^\circ/2\theta$ to $64^\circ/2\theta$ with a Phillips diffractometer equipped with a graphite monochromator and a theta-compensating divergence slit. For the semiquantitative evaluation of the data, the integrated intensities of the analytical reflections of the minerals were measured. For the clay analyses, carbonate phases were removed from the sample of the Green River Formation by digestion in a 1-N Na-acetate solution buffered at pH 5 with glacial acetic acid. This treatment dissolves carbonates without damaging the clays as would any harsher acid treatment at lower pH values. Stable suspensions were prepared from the powders of the Chattanooga and Alum shales and the insoluble residue of the Green River Formation sample. Oriented slides were made from the $<2 \mu\text{m}$ fractions using these suspensions. The slides were x-rayed ($2^\circ/\theta$ to $45^\circ/\theta$) after drying at room temperature. Subsequently, the same slides were saturated with ethylene glycol overnight and x-rayed again.

3.1.2 Electron Microscopy

The clay fractions of the samples were examined in both transmission electron microscopy (TEM) and energy-dispersive spectral analysis (EDS) modes at 100 keV potential using a JEM-100 CX Electron

Microscope. The clay samples were thoroughly dispersed in distilled water using a 20- to 30-m ultrasonic treatment. The suspension was further diluted in a 0.007% tertiary butylamine solution, which is known to reduce the surface tension forces between clay particles during the drying of the suspension. A drop of this suspension was air-dried on a copper grid that had been coated with a formvar film. The copper grids with the clay particles on them were then coated with carbon. The EDS analyses of the clay particles were carried out with a KEVEX 8000 Microanalyzer equipped with an ultra-thin window Si(Li) detector that has a high detection efficiency for light-atomic-weight elements down to carbon.

3.2 RESULTS

3.2.1 Chattanooga Shale

According to the X-ray diffraction data, quartz and illite are the predominant minerals present in the Chattanooga Shale occurring at levels of approximately 25 to 30 wt % each. Pyrite occurs in appreciable quantities ranging from 5 to 10 wt %. Small quantities (<5 wt %) of chlorite, K feldspar, and anhydrite are also found in the shale. In addition, calcite is macroscopically visible as vein fillings. The amount of calcite, hence the intensity of the calcite reflections, varies with the selection of the sample in relation to the calcite veins.

Samples that were heat treated for 24 h show no significant thermal alteration up to 400°C, except for the sharpening of the basal reflection of the illite. The interplanar spacing of the 001-reflection shows little change (Table 3.1). The X-ray data also indicate that the illite present contains negligible amounts of expandable layers (smectite) in its structure.

Significant changes in the shale mineralogy are observed after heating at 500 and 600°C. A distinct 13.8-Å reflection of chlorite appears after the heat treatment at 500°C, while the 7.14- and 3.55-Å reflections disappear. This behavior confirms the presence of

Table 3.1. Interplanar spacing of the 001-reflection of illite as a function of heat treatment for 24 h

Temperature (°C)	d_{001} (Å)
Ambient	10.09
100	10.09
200	10.03
300	10.03
400	10.12
500	9.94
600	10.05

chlorite in the shale. The heat treatments at 500 and 600°C cause the total oxidation of pyrite to hematite; the latter phase is characterized by strong reflections at 3.67, 2.698, 2.514, 2.200, 1.841, and 1.691 Å.

Electron microscopic examination of the original shale and its products from heat treatment shows that the illite retains its morphological, structural, and chemical features. Illite particles occur as subhedral flakes and platelets that range in size from 0.05 to 2.0 μm . Typical illite particles in the sample are shown in Figs. 3.1-3.6. The illite flakes generally have a dense core surrounded by thin rims. Digital scanning TEM imaging gives a more illustrative representation of the particle topography than the conventional black-white analog TEM images (Fig. 3.5). The overgrowths appear as subrounded (dislike) domains along the edges of the flakes and they are also visible at the basal surfaces. A closeup view of the dislike domains is shown in Fig. 3.2. These domains range in size from a few hundredths of a μm up to 0.5 μm . The illite flakes are coated with dense precipitates of an iron oxide that vary in shape from minute grains to laths and hexagonal platelets. Figure 3.4 illustrates typical iron-oxide precipitates in the illite flakes.



Fig. 3.1. Chattanooga Shale; 44,000X; untreated. Typical illite crystallite displaying a mosaic of tiny domains. The illite crystallite is $\sim 2 \mu\text{m}$ in size and subrounded in form.

ORNL-PHOTO-2024-88

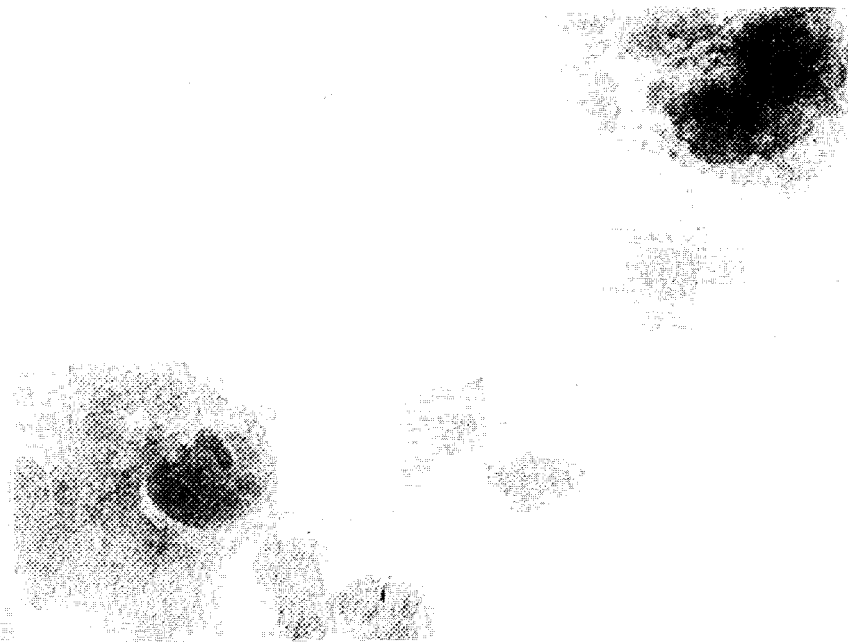


Fig. 3.2. Chattanooga Shale; 135,000X; untreated. A closeup view of individual domains in the mosaic of illite crystallites. These domains are subrounded and $< 0.05 \mu\text{m}$ in size.

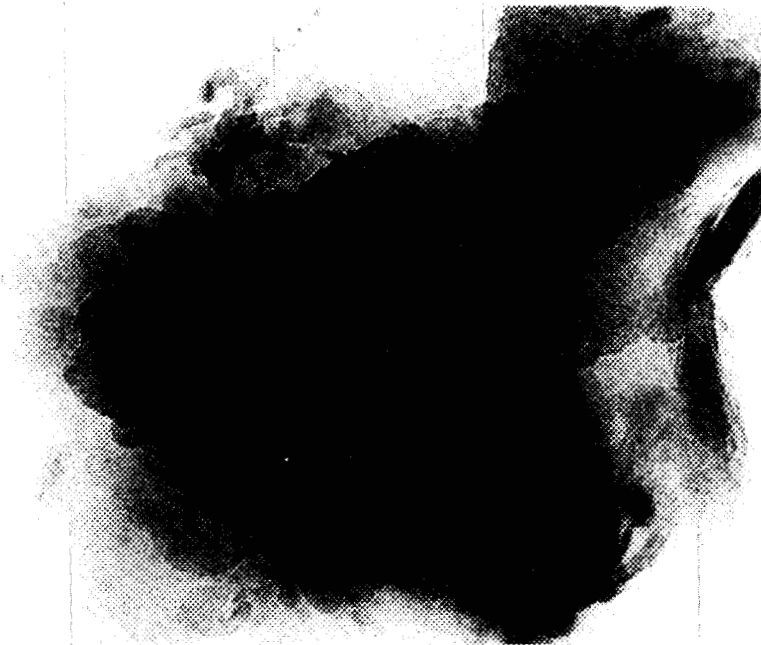


Fig. 3.3. Chattanooga Shale; 65,000X; untreated. A dense aggregate of illite that may have some smectite as mixed-layers in its structure or silica precipitates (based on X-ray spectral data).

ORNL-PHOTO-2028-88

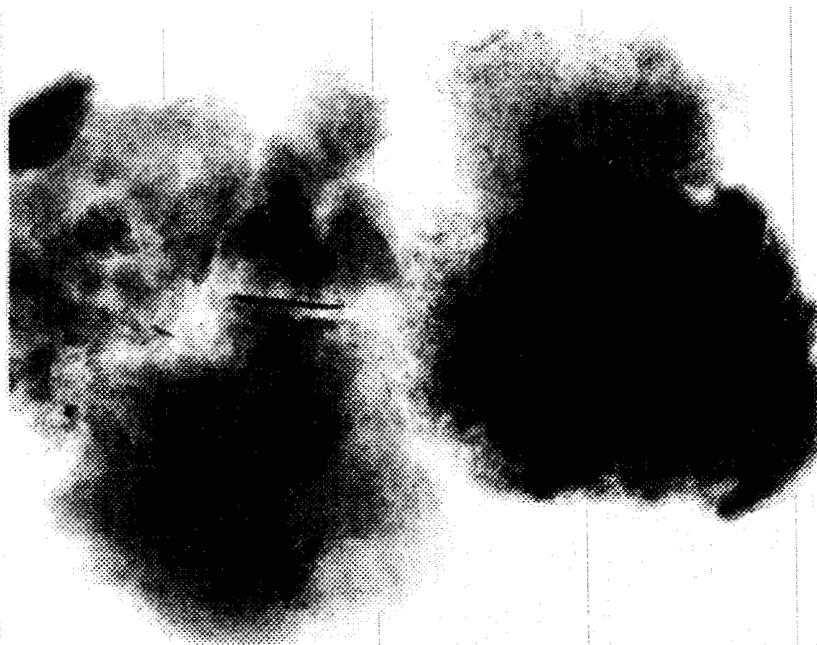


Fig. 3.4. Chattanooga Shale; 45,000X; untreated. Detrital illite flakes with subrounded forms and dense iron-oxide coatings. The iron-oxide coatings range in size from 0.01 to 1 μm .

ORNL-PHOTO-01991-88

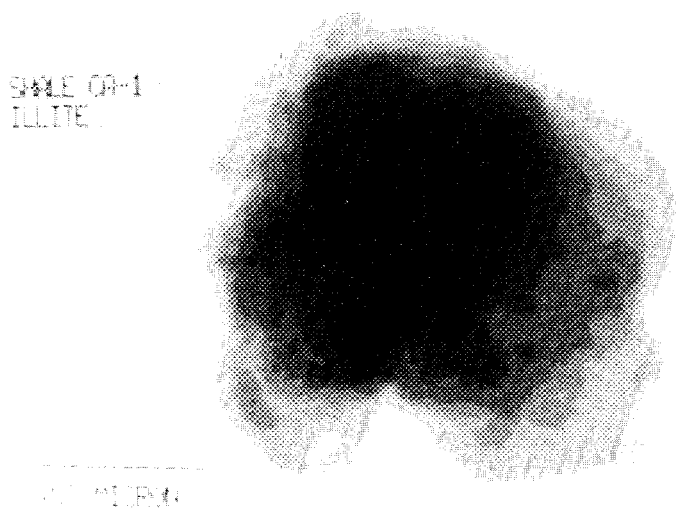


Fig. 3.5. Chattanooga Shale; untreated. Digital image of an illite particle that illustrates the internal structure and the topography of the platelet.

ORNL-PHOTO-2030-88

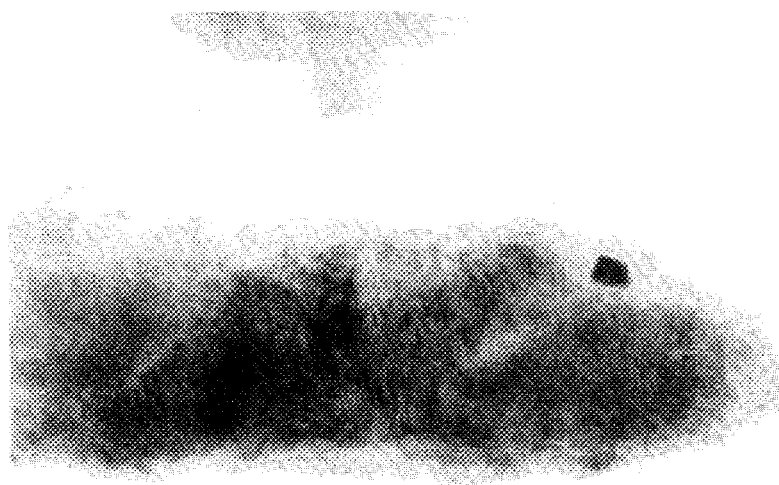


Fig 3.6. Chattanooga Shale; 30,000X; untreated. An elongated illite flake with subrounded edges and with the approximate dimensions of 0.5 X 1.5 μm .

The typical chemistry of the illite particles, based on EDS X-ray spectra, can be represented by the major elements Si, Al, O, and K, with minor amounts of Mg and Fe. X-ray mapping provides a view of the distribution of these elements over the clay particles and suggests a uniform distribution of Si, Al, Fe, and K. X-ray spectral data were obtained from several illite particles and are compared with data for a standard illite (Silver Hill) in Table 3.2. The spectral data are listed as intensity ratios with respect to the intensity of the K line of silicon. The X-ray spectral data of the illite particles in the Chattanooga sample are similar to the spectral data from the Silver Hill illite. The spectral intensities are converted to atomic ratios to obtain the chemical composition of the illite particles. These atomic ratios are listed in Table 3.3 and indicate that the illites in the Chattanooga Shale are similar in chemical composition to the Silver Hill illite. The heat treatments up to 600°C do not cause any apparent changes in these ratios. In addition to illite, there are "mica" particles present that are distinguishable from illites by their higher concentrations of Al and K (see Table 3.3).

No morphological or chemical changes are observed for illite particles after the heat treatments. Figure 3.7 shows aggregates of illite flakes containing sporadic iron-oxide coatings. A typical chemical composition of the illite flake after the 100°C heat treatment is shown in Tables 3.2 and 3.3. Similarly, typical illite flakes that were previously heated at 300°C are illustrated in Fig. 3.8 and 3.9, and their chemical composition is listed in Table 3.3. Subrounded illite flakes with dense detrital cores carry various amounts of iron-oxide coatings. The iron oxide shown in Fig. 3.8 has a lathlike habit and is approximately 0.5 μm long. The iron oxide precipitates on the illite (mica) shown in Fig. 3.9 are minute granules that represent the early nucleation stage of iron oxide on the illite substrate. Transparent (thin) and denser illite flakes with subrounded forms are shown in Figs. 3.10 and 3.11 after the heat treatment of the shale at 400°C. Similar illite flakes are also observed after heating the shale to 500°C (Fig. 3.12). Large amounts of dense iron oxide (hematite) are

Table 3.2. X-ray spectral intensity data on Chattanooga Shale
(intensity ratios relative to the K line of silicon)

Mg	Al	Si	K	Fe	Particle	Heat-treatment temperature (°C)
0.04	0.49	1.00	0.26	0.12	S.H. illite ^a	ambient
0.05	0.50	1.00	0.22	0.07	illite (see Fig. 3.1)	ambient
0.08	0.49	1.00	0.20	0.05	illite (see Fig. 3.3)	ambient
0.06	0.59	1.00	0.25	0.09	illite (see Fig. 3.6)	ambient
0.06	0.52	1.00	0.21	0.12	illite (see Fig. 3.7)	100
0.03	0.40	1.00	0.19	0.09	illite (see Fig. 3.8)	300
0.09	0.63	1.00	0.37	0.11	mica (see Fig. 3.9)	300
0.08	0.56	1.00	0.20	0.13	illite (see Fig. 3.10)	400
0.04	0.59	1.00	0.29	0.05	mica (see Fig. 3.11)	400
0.06	0.51	1.00	0.17	0.05	illite (see Fig. 3.12)	500
0.05	0.69	1.00	0.16	0.05	illite (see Fig. 3.14)	600
0.08	0.56	1.00	0.24	0.05	mica (see Fig. 3.15)	600

^astandard Silver Hill illite sample with the composition
(K_{0.68}Na_{0.01})(Al_{1.34}Si_{3.66})(Al_{1.39}Fe_{0.33}Mg_{0.28})O₁₀(OH)₂

Table 3.3. Elemental ratios (relative to Si) in illite particles as
obtained from X-ray spectra in Table 3.2

Mg	Al	Si	K	Fe	Particle	Heat-treatment temperature (°C)
0.06	0.48	1.00	0.19	0.09	S.H. illite ^a	ambient
0.07	0.49	1.00	0.16	0.05	illite (see Fig. 3.1)	ambient
0.11	0.48	1.00	0.15	0.04	illite (see Fig. 3.3)	ambient
0.09	0.58	1.00	0.19	0.07	illite (see Fig. 3.6)	ambient
0.06	0.52	1.00	0.21	0.12	illite (see Fig. 3.7)	100
0.04	0.39	1.00	0.14	0.07	illite (see Fig. 3.8)	300
0.13	0.62	1.00	0.27	0.08	mica (see Fig. 3.9)	300
0.11	0.55	1.00	0.15	0.09	illite (see Fig. 3.10)	400
0.06	0.58	1.00	0.22	0.04	mica (see Fig. 3.11)	400
0.09	0.50	1.00	0.13	0.04	illite (see Fig. 3.12)	500
0.07	0.68	1.00	0.12	0.04	illite (see Fig. 3.14)	600
0.11	0.55	1.00	0.18	0.04	mica (see Fig. 3.15)	600

^astandard Silver Hill illite sample with the composition
(K_{0.68}Na_{0.01})(Al_{1.34}Si_{3.66})(Al_{1.39}Fe_{0.33}Mg_{0.28})O₁₀(OH)₂

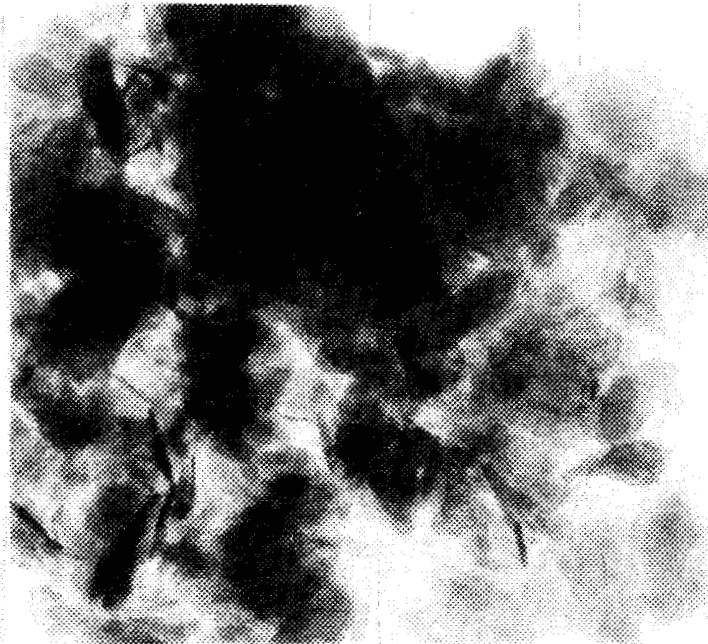


Fig. 3.7. Chattanooga Shale; 65,000X; 100°C heat treatment. An aggregate of clay particles consisting of detrital illite flakes and a few chlorites with sporadic iron-oxide coatings (after heating at 100°C for 24 h).

ORNL-PHOTO-2031-88

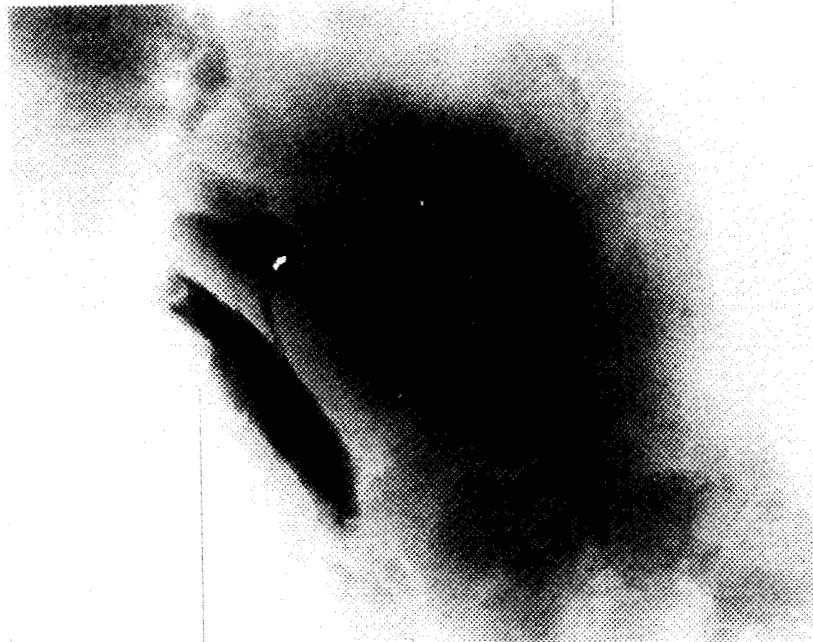


Fig. 3.8. Chattanooga Shale; 65,000X; 300°C heat treatment. Typical illite flakes and dense iron-oxide coatings in the shale after heat treatment at 300°C for 24 h. No morphological or structural changes are visible on the illite flakes.

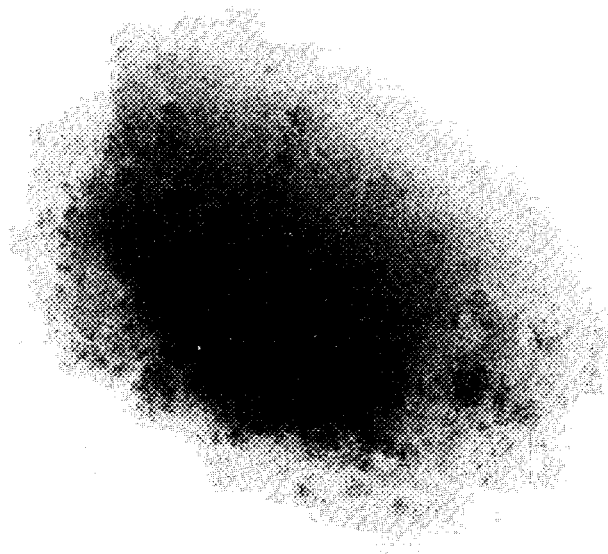


Fig. 3.9. Chattanooga Shale; 135,000X; 300°C heat treatment. Illite flake with a subrounded form and iron-oxide precipitates on the surface.

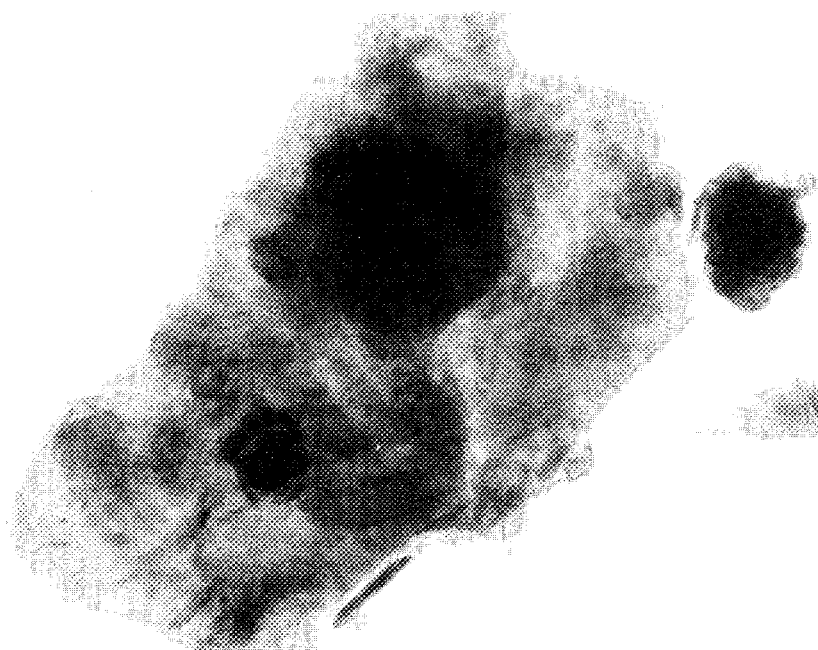


Fig. 3.10. Chattanooga Shale; 45,000X; 400°C heat treatment. A typical detrital flake of illite (3.0 μm).

ORNL-PHOTO-2036-88

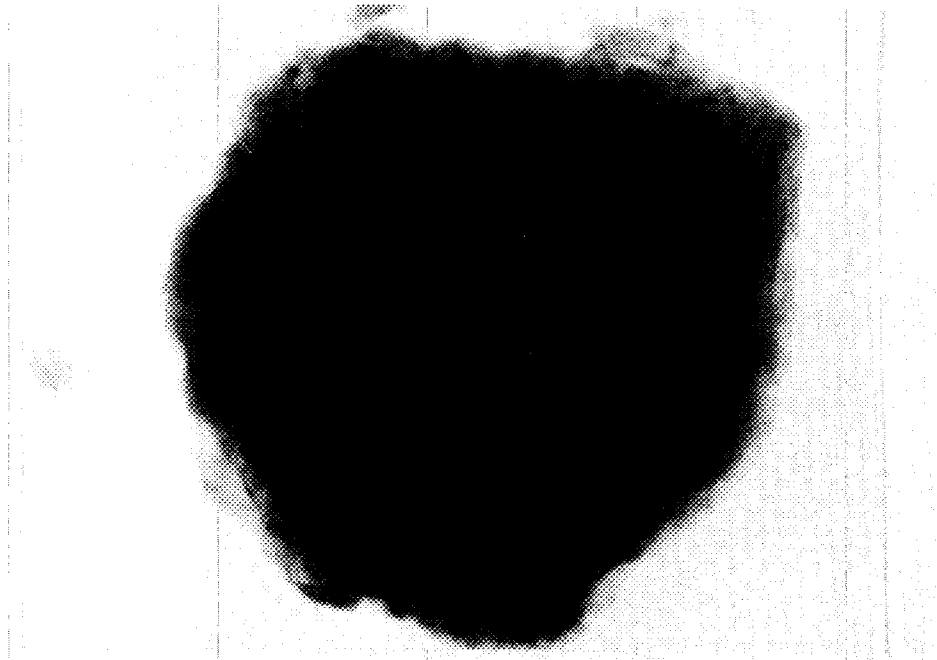


Fig. 3.11. Chattanooga Shale; 35,000X, 400°C heat treatment. A dense and subrounded flake of detrital illite.

ORNL-PHOTO-2033-88

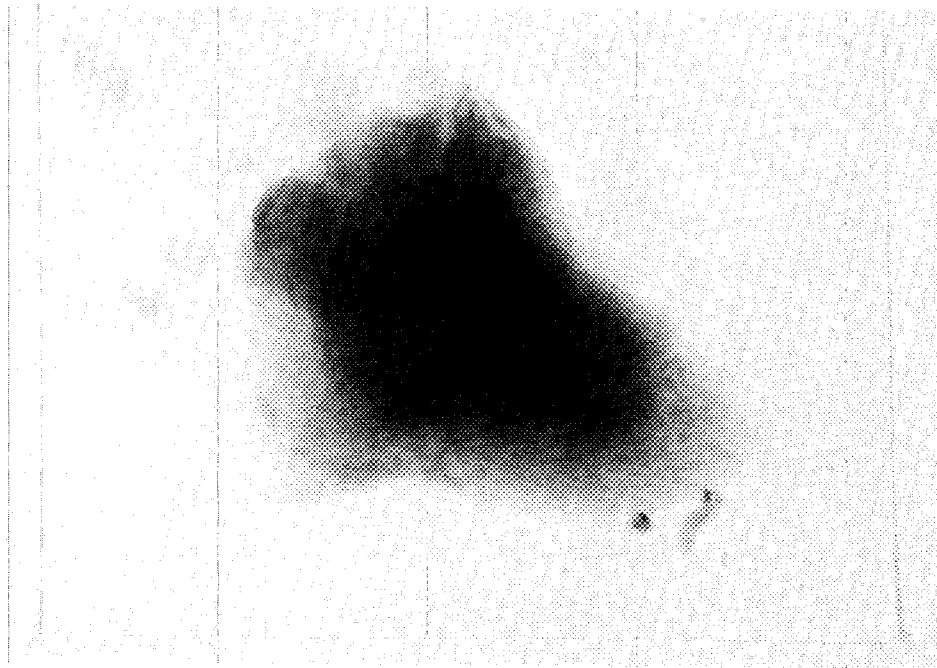


Fig. 3.12. Chattanooga Shale; 45,000X; 500°C heat treatment. Typical detrital illite flake that remained unaltered during the 500°C heat treatment.

formed at 500°C, as shown in Fig. 3.13. In the latter figure, hematite is observed both as hexagonal platelets up to 0.2 μm diam and as dense coatings on the surface of illite flakes. Similar iron-oxide particles are displayed in Figs. 3.14-3.16 for the shale that was heat treated at 600°C. The illite flakes, however, maintain their morphological and structural characteristics even at 600°C.

3.2.2 Alum Shale

The mineralogical composition of the Alum Shale is similar to that of the Chattanooga Shale. Quartz and illite are approximately equal in amounts and comprise around 60 wt % of the rock. Pyrite is found in appreciable amounts (~10 wt %), and K feldspar, calcite, anhydrite, chlorite, and kaolinite occur in small (<5 wt %) quantities.

Illite occurs as subhedral flakes, indicating a detrital origin. Typical illite particles are displayed in Figs. 3.17 and 3.18. They consist of flakes up to 0.4 μm diam and they usually are coated with minute, dense grains of iron-oxide precipitates. Digital imaging again reveals the gradual increase in thickness from the rims toward the center of the illite particles (Fig. 3.19). This image also shows the complex topography of the illite surface having two dense sections. An X-ray spectrum obtained from this illite indicates that the major elemental components are Si, Al, O, and K, while Mg and Fe are minor constituents. X-ray mapping of the illite particle for Si, Al, K, and Fe shows a uniform distribution of these elements over the surface of the particle. The X-ray spectra obtained from illite particles in the original, untreated sample and from samples that were heat treated are summarized in Table 3.4 and corresponding atomic ratios are listed in Table 3.5. The X-ray spectra illustrate that the illites in the Alum Shale are similar in composition to the standard Silver Hill illite. Furthermore, no significant changes occurred in the chemistry of the illites during the heat treatment.

Heat treatment up to 400°C does not affect the mineral components of the shale except for enhancing and sharpening the basal X-ray diffraction (XRD) reflections of illite. This result is probably

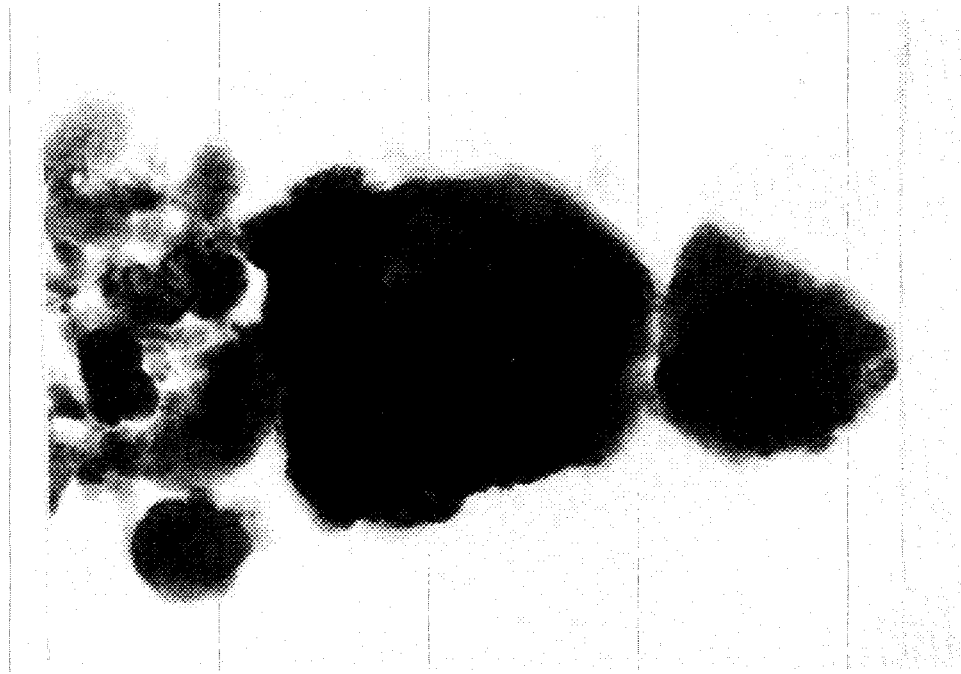


Fig. 3.13. Chattanooga Shale; 90,000X; 500°C heat treatment. Dense hematite precipitates on an illite substrate formed during the oxidation of pyrite.

ORNL-PHOTO-2034-88

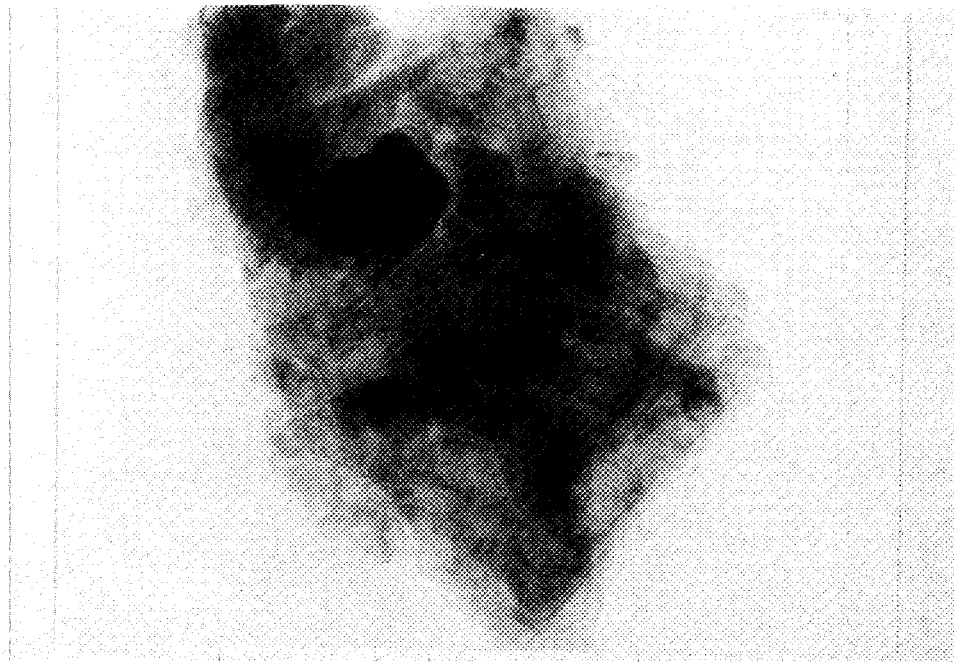


Fig. 3.14. Chattanooga Shale; 35,000X; 600°C heat treatment. Typical detrital illite flake $-3.0 \mu\text{m}$. Note the $-0.5\text{-}\mu$ dense crystallite of iron oxide that formed on the surface of the illite.



Fig. 3.15. Chattanooga Shale; 27,000X; 600°C heat treatment. Dense, rounded illite flake about $\sim 4.0 \mu\text{m}$ with dense iron-oxide precipitates on the surface.

ORNL-PHOTO-2039-88

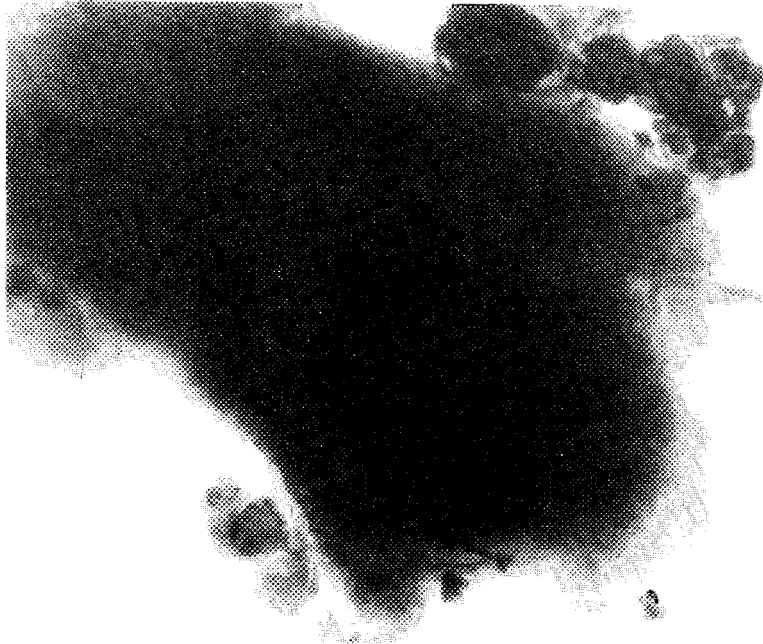


Fig. 3.16. Chattanooga Shale; 35,000X; 600°C heat treatment. Illite flake surrounded by dense iron-oxide platelets with hexagonal forms. Hematite crystallites form at 600°C and range from 0.1 to $0.5 \mu\text{m}$.

ORNL-PHOTO-2040-88



Fig. 3.17. Alum Shale; 27,000X; untreated. Typical illite flakes with subrounded outlines and minute iron-oxide precipitates.

ORNL-PHOTO-2042-88



Fig. 3.18. Alum Shale; 27,000X; untreated. Illite flakes with dense iron-oxide coating.

ORNL-PHOTO-01940-88

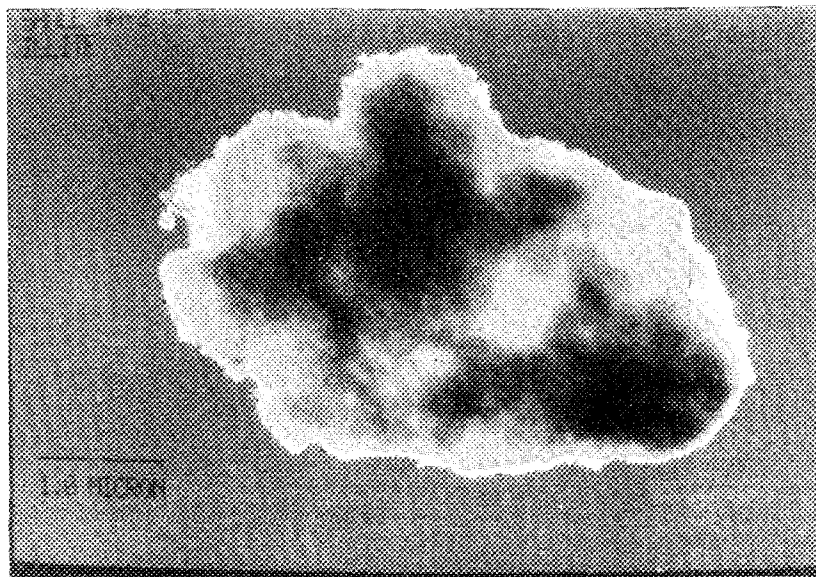


Fig. 3.19. Alum Shale; untreated. Digital image of an illite particle displaying its internal structure and topographic features.

Table 3.4. X-ray spectral intensity data on Alum Shale (intensity ratios relative to the K line of silicon)

Mg	Al	Si	K	Fe	Particle	Heat-treatment temperature (°C)
0.04	0.49	1.00	0.26	0.12	S.H. illite ^a	ambient
0.04	0.52	1.00	0.21	0.15	illite (see Fig. 3.18)	ambient
0.09	0.51	1.00	0.35	0.07	illite (see Fig. 3.21)	600
0.03	0.63	1.00	0.27	0.11	illite (see Fig. 3.20)	600
0.05	0.58	1.00	0.27	0.04	illite (see Fig. 3.17)	ambient

^astandard Silver Hill illite sample with the composition $(K_{.68}Na_{.01})(Al_{.34}Si_{3.66})(Al_{1.39}Fe_{.33}Mg_{.28})O_{10}(OH)_2$

Table 3.5. Elemental ratios (relative to Si)
in the illite particles in Table 3.4

Mg	Al	Si	K	Fe	Particle	Heat-Treatment temperature (°C)
0.06	0.48	1.00	0.19	0.09	S.H. illite ^a	ambient
0.06	0.51	1.00	0.16	0.11	illite (see Fig. 3.18)	ambient
0.13	0.50	1.00	0.26	0.05	illite (see Fig. 3.21)	600
0.04	0.62	1.00	0.20	0.08	illite (see Fig. 3.20)	600
0.07	0.57	1.00	0.20	0.03	illite (see Fig. 3.17)	ambient

^astandard Silver Hill illite sample with the composition
(K_{0.68}Na_{0.01})(Al_{1.34}Si_{3.66})(Al_{1.39}Fe_{0.33}Mg_{0.28})O₁₀(OH)₂

caused by the removal of residual water molecules from the interlayer regions in the illite. After heat treatment at 500°C for 24 h, the 14.1-Å reflection of chlorite appears with a simultaneous reduction in the intensity of the 7.17-Å reflection. Thus, the heat treatment clearly reveals the presence of kaolinite and chlorite in shale. The main high-temperature reactions take place at 500 to 600°C and involve the oxidation of pyrite to hematite. Typical illite particles maintain their integrities, as illustrated in Figs. 3.20 and 3.21. Dense patches composed of hematite crystallites are often located on the illite substrates (Fig. 3.20), but they also occur as isolated precipitates separate from the illite.

3.2.3 Green River Formation

Carbonates (40 to 45 wt %) and quartz (15 to 20 wt %) are the predominant mineral phases of the sample of Green River Formation. The carbonates are composed mainly of ankerite, Ca(Fe,Mg,Mn)(CO₃)₂, which is characterized by its strong reflection at 2.895 Å. Calcite is found in only small quantities (<5 wt %). K feldspar and plagioclase occur in small amounts (~5-10 wt %). Illite is the only clay mineral present and it occurs in rather insignificant quantities (<3 wt %).

The heat treatment does not cause any significant mineral reactions except for the formation of hematite at 500°C and above.

ORNL-PHOTO-2035-88

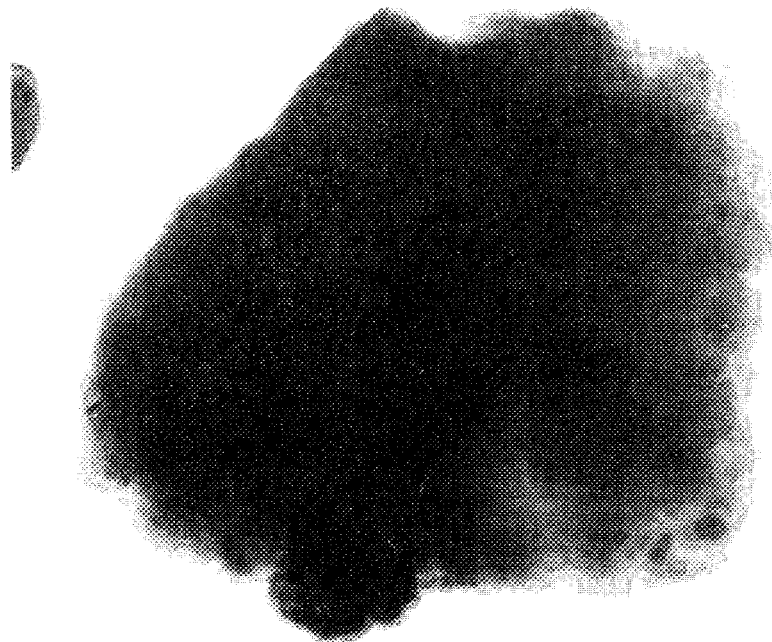


Fig. 3.20. Alum Shale; 35,000X; 600°C heat treatment. Subrounded illite flake with dense clusters of iron-oxide precipitates that form during heat treatment.

ORNL-PHOTO-2041-88



Fig. 3.21. Alum Shale; 27,000X; 600°C heat treatment. Typical illite flake that remains unaltered during the heat treatment at 600°C.

Because the pyrite content of the shale is negligible, the source of the iron for the formation of hematite may be the iron-oxide coatings on the clays and/or the decomposition of ankerite in small quantities.

3.3 DISCUSSION

A combination of XRD and electron microscope techniques were used to characterize the mineralogic properties of the Chattanooga Shale, the Alum Shale, and the Green River Formation, both before and after heat treatments. The mineralogic composition of these samples is reasonably consistent with results from Lee, Hyder, and Alley (1988). Heat treatments (24 h) up to 600°C result in minimal mineralogic changes, with the exception of the oxidation of pyrite to hematite. Illites, the predominant clay mineral in these shales, were found to be similar to the standard Silver Hill illite and did not undergo significant alteration during the heat treatments. Iron oxides typically occurred as coatings on the surface of the illites. This mode of occurrence may be important to consider when interpreting results from sorption experiments. The oxide coating may interfere with ion-exchange reactions of radionuclides. The coatings themselves may also act as strong adsorbents for some radionuclides under certain geochemical conditions (e.g., basic pH conditions); therefore, further detailed study using these microanalytical techniques combined with autoradiography could yield some useful results.

4. ANALYSIS OF ORGANIC MATTER IN SHALES BY FLUORESCENCE MICROSCOPY

Organic petrology is the description and classification of the origin, occurrence, structure, and history of the fossil organic matter preserved in sedimentary rocks; and it is developing from fundamental principles of coal petrology. Among the basic concepts is the "maceral concept" proposed by Stopes (1935), who defined the individual organic constituents in coal as macerals. In coals and sedimentary rocks, three maceral groups are identified that occur in varying amounts. The liptinites are derived from leaf cuticle, spores, pollen, plant waxes, fats, oils, and resins. The vitrinites are preserved woody tissue of plants. The inertinite macerals consist of woody matter that has been altered by oxidation, mouldering, and biological attack. Spackman (1958) proposed that these macerals are discrete substances possessing diagnostic chemical and physical properties. Although properties of the individual macerals are the topics of current studies, it is clear that the behavior of bulk coals and rock samples in a given technological process is, in a large part, governed by the relative maceral blend.

Advancing technology in the field of coal petrology has allowed researchers to identify new and a greater variety of macerals in coals and sedimentary rocks. Utilizing fluorescence microscopy, Teichmüller (1974) identified liptinites not easily observed in white light. Spackman, Davis, and Mitchell (1976) later verified their existence in North American coals. Crelling (1983) reported maceral structures and textures in western American coals using fluorescence microscopy.

Another important property of preserved organic matter is the degree to which it has been altered after burial. Here, near parallel terms are used to describe the evolution of organic matter as a function of temperature and pressure over a period of geologic time. Coalification is the evolution of peat through the stages of lignite, subbituminous coal, bituminous coal, anthracite, and meta-anthracite. Similarly, maturation is the term used to describe the evolution of dispersed sedimentary organic matter after deposition. Rank is the

position of a coal or sedimentary rock sample in this progression and is measured petrographically by vitrinite reflectance. Vitrinite reflectance is the preferred indicator because it varies linearly during organic metamorphism (McCarthy and Teichmüller 1972; Smith and Cook 1980). Thus, as rank increases, vitrinite reflectance increases.

Changes in liptinite fluorescence properties have been studied more for coals than for sedimentary rocks. Early work showed a shift to the longer wavelengths in sporinite spectra as a function of increasing coal rank (Ottenjann, Teichmüller, and Wolf 1975). In a more recent account, Teichmüller and Durand (1983) reported the fluorescence coalification patterns of sporinite, cutinite, resinite, and fluorinite macerals. Landis and Crelling (1985) reported the coalification trends of secondary fluorescing macerals well beyond previously suspected limits.

From the body of literature over the last several decades, it has become clear that (1) preserved sedimentary organic matter is seldom a homogenous assemblage and (2) the amount, type, and rank of organic matter must be characterized to predict bulk sample behavior. Thus, the objective of this work was to characterize the petrographic properties of the Alum Shale, the Chattanooga Shale, and the Green River Formation. Specific goals were to

1. determine the maceral composition of these shales in both reflected white and blue light, and
2. measure the petrographic variation of these shales as a function of controlled thermal alteration

4.1 METHODS

The fluorescence spectroscopic analyses comprise both quantitative and semiquantitative reflected white- and blue-light microscopy. For all petrographic work, the shale samples were bound in epoxy, forming 2.5-cm-diam pellets. These pellets were polished to a 0.05- μm finish. The maceral analyses were performed using a Leitz MPV III Orthoplan microscope at 500X. A mechanical stage was used to advance the pellet so that the entire surface was surveyed (increments were 0.3 mm in the

x-direction, 1.5 mm in the y-direction). One set of 500 points was counted in both white and blue light for the identification of the various macerals. Mean random vitrinite reflectance was determined by averaging no more than 25 individual readings. Histogram plots were constructed to evaluate the reflectance distribution, and in some cases the dearth of vitrinite macerals produced an average reflectance from fewer than 25 readings.

The quantitative fluorescence analyses consisted of both spectral and temporal data acquisition. The number of spectra acquired per sample of shale depended upon the abundance of fluorescing macerals present, the fluorescence intensity, and the nature of the liptinite distribution; thus, the number of spectra varied from five to ten. The excitation wavelength (365 nm) was provided by a 100-W Hg lamp. The spectral scan range covered much of the visible spectrum (420 to 720 nm), and the relevant parameters extracted from any one spectrum were the spectral maximum and quotient. The spectral maximum is defined as the wavelength of maximum intensity, and the spectral quotient is the ratio of the intensity at 650 nm to the intensity at 500 nm.

The temporal analyses employed near-uv excitation (395 nm) from a nitrogen-pumped, pulsed, tunable-dye laser. The details of this apparatus have been described previously (Landis et al., 1987). Essentially, the fluorescence decay is acquired between each excitation pulse, averaged over a user-defined sample number, and then stored for later use. For each sample offering sufficient fluorescence intensity, decay curves were gathered at the emission wavelength of maximum intensity. From each average pulse, the characteristic lifetimes, the percent contributions, and the Einstein A-coefficients were obtained.

4.2 RESULTS

4.2.1 Macerals

To better characterize the maceral composition of these shales, a combined maceral analysis consisting of both blue- and white-light point counts was completed. The combined maceral analysis was first suggested by Spackman, Davis, and Mitchell (1976) who recommended it for coals with a liptinite fraction greater than 5 vol %. It was intended to better estimate the amount of various liptinites in coals in the vitrinite groundmass. Similarly, the combined analysis was completed here to better contrast the liptinites and the mineral matrix.

The results of both maceral analyses for the untreated samples are presented in Table 4.1. It is evident that the liptinites dominate the maceral distribution for all these shales, but detectable quantities of vitrinite and inertinite are also present (see Fig. 4.1-4.3). Nonindigenous vitrinite or second-cycle vitrinite is most common in the Chattanooga Shale, suggesting periodic terrestrial influx. For all three shales, the inertinites total <2 vol %.

The most abundant macerals in all three shales are the liptinites. In these shales, alginite, bituminite, and liptodendrinite are the dominant constituents. The Chattanooga Shale contains the most diverse liptinite assemblage, with trace amounts of resinite, sporinite, and amorphous vug fillings associated with alginite and liptodendrinite. Chattanooga alginites offer strong yellow fluorescence, vary in length (10 to 30 μm), and commonly rest parallel to sedimentary bedding (Fig. 4.4). They total approximately 8 vol % of the Chattanooga Shale. The weakly fluorescent groundmass is also rather conspicuous (9 vol %) but probably indicates the interaction of submicroscopic organic matter with groundmass minerals.

The maceral assemblage is much less diverse for the Alum and Green River Formation shales. The Alum Shale liptinite assemblage is characterized by high alginite and bituminite percentages. The fluorescence is characterized by weak yellowish-orange intensities that

Table 4.1. Pairs of white- and blue-light maceral analyses of Chattanooga, Alum, and Green River Formation shales showing their compositional diversity and improved detection of liptinites in blue-light (all measurements are in volume percent)

Chattanooga Shale												
	<u>Inertinite</u>		<u>Vitrinite</u>			<u>Liptinite</u>						
	<u>SemiFus</u>	<u>Fus</u>	<u>2nd</u>	<u>1st</u>	<u>Gran.Vit.</u>	<u>Alginite</u>	<u>Resinite</u>	<u>Sporinite</u>	<u>Liptodet.</u>	<u>Amorph.</u>	<u>FluorGroundmass</u>	<u>TMOC</u>
White light	0.6	0.8	1.0	0.5	1.8	2.4						7.2
Blue light						8.2	0.4	Trace	3.0	0.8	9.6	22.0

Alum Shale										
	<u>Inertinite</u>		<u>Vitrinite-like</u>			<u>Liptinite</u>				
	<u>SemiFus</u>	<u>Fus</u>	<u>2nd</u>	<u>1st</u>	<u>Gran.Vit.</u>	<u>Alginite</u>	<u>Bituminite</u>	<u>Resinite</u>	<u>FluorGroundmass</u>	<u>TMOC</u>
White light	0.2			0.2	3.6	6.8	9.0			17.4
Blue light						13.6	7.6	0.4	10.0	31.6

Green River Formation									
	<u>Inertinite</u>		<u>Vitrinite</u>			<u>Liptinite</u>			
	<u>SemiFu</u>	<u>Fus</u>	<u>2nd</u>	<u>1st</u>	<u>Gran.Vit.</u>	<u>Alginite</u>	<u>Amorph.</u>	<u>TMOC</u>	
White light	0.2	1.0		1.5		0.2		3.0	
Blue light						3.5	8.8	12.8	

^aAbbreviations: SemiFus = seimifusinite; Fus = fusinite; 2nd = secondary (nonindigenous) vitrinite; 1st = primary (indigenous) vitrinite; Gran.Vit. = granular vitrinite; Liptodet. = liptodendrinite; Amorph. = amorphous vug fillings; FluorGroundmass = fluorescent groundmass; TMOC = total microscopic organic matter.

ORNL-PHOTO-02113-88

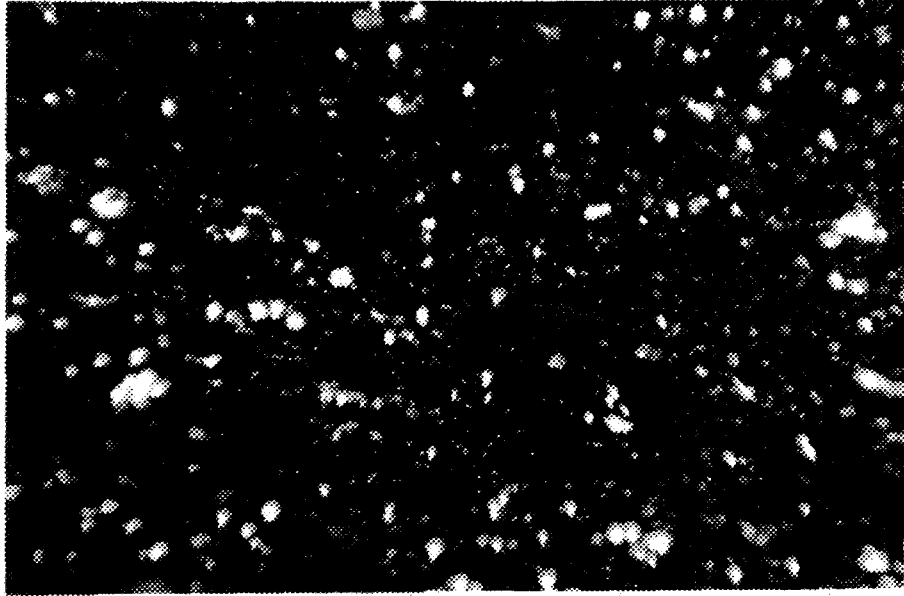


Fig. 4.1. Photomicrograph of Alum Shale vitrinite like organic material in a mineral matrix including conspicuously bright pyrite (reflected white light at 750X).

ORNL-PHOTO-02112-88



Fig. 4.2. Photomicrograph of Green River Formation vitrinite (reflected white light at 750X).

ORNL--PHOTO--02111--88

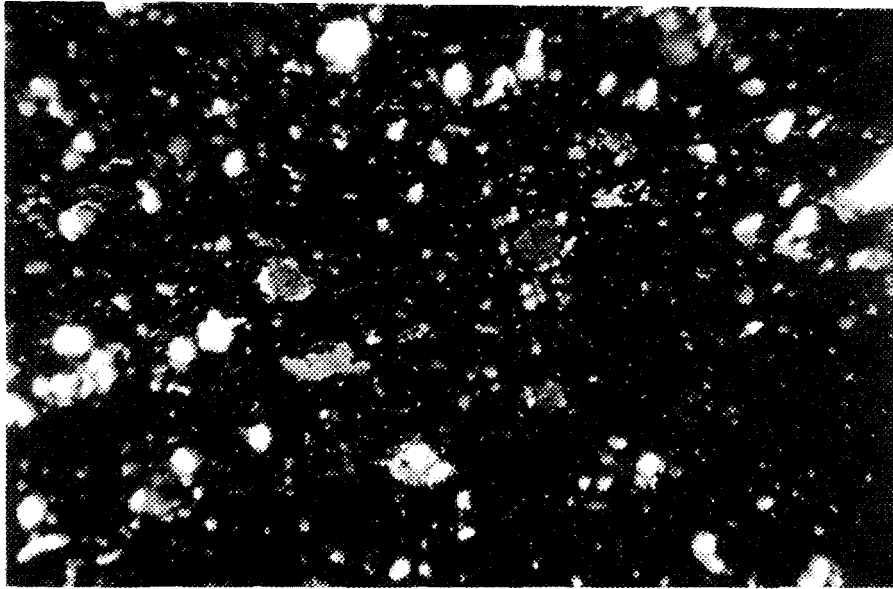


Fig. 4.3. Photomicrograph of Chattanooga Shale vitrinite in mineral groundmass (reflected white light at 750X).

ORNL--PHOTO--02110--88

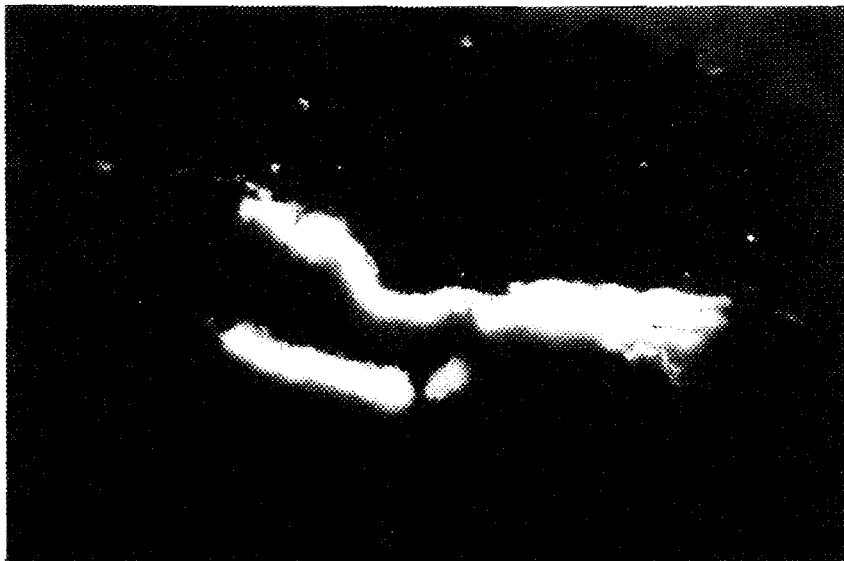


Fig. 4.4. Photomicrograph of untreated Chattanooga Shale alginite. Note the strong fluorescence of the alginite and the nonfluorescence of the groundmass (reflected blue light at 750X).

increase as a function of continued uv radiation (Fig. 4.5). This increase in fluorescence intensity as the maceral is exposed to uv excitation is called positive alteration (Ottenjann, Teichmüller, and Wolf 1975). The alginite of the Alum Shale does not occur as discrete bodies, as in the Chattanooga Shale, but as poorly preserved bodies that tend to merge into the bituminite. This lack of morphological integrity for both the alginite and bituminite suggests that the bituminite may be a product of altered algal bodies. Indeed, their fluorescence properties are similar. Like the Chattanooga Shale, a weakly fluorescent orange groundmass totaling approximately 10 vol % can also be observed. This fraction probably relates to intimately associated minerals and submicroscopic organic material.

The Green River Formation shale sample contains less fluorescent microscopic material than the other two organic-rich shales. Further, the fluorescent substances are localized in enriched laminae (Fig. 4.6) as orange amorphous vug and apophyses fillings. Well-preserved alginite occurs in trace amounts.

Table 4.1 illustrates how the blue-light maceral analysis permits an improved estimate of the liptinite content. A several-fold increase in detectable microscopic organic matter is obtained via blue-light inspection of these liptinitic shales. Further, the relatively inconspicuous alginite is much more noticeable in blue light for all the samples. That the Alum Shale bituminite is better counted in white light relates to its weak fluorescence intensity. Thus, the combined use of white- and blue-light maceral analysis yields

1. a more complete examination of the maceral assemblage of each shale,
2. a more accurate liptinite estimation (volume percent), and
3. the nature of liptinite associations and occurrences in a particular sample.

4.2.2 Vitrinite Reflectance Analysis

Mean random vitrinite reflectances were obtained from samples that did not combust during the heat treatments and that represent a

ORNL-PHOTO-02109-88

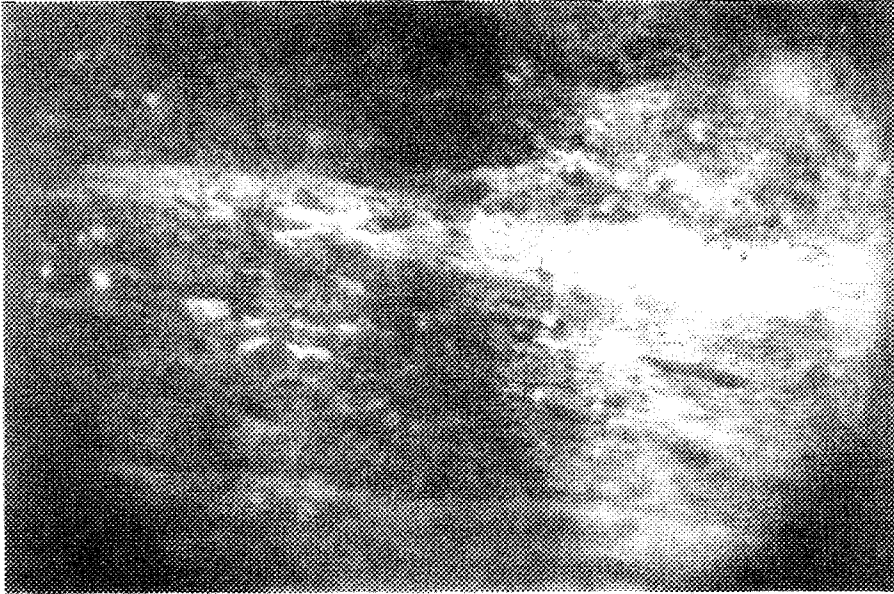


Fig. 4.5. Photomicrograph of positive alteration of Alum Shale liptinite. Note the stronger intensity on the right side of the micrograph as a result of 3 min of continuous uv excitation (reflected blue light at 250X).

ORNL-PHOTO-02108-88

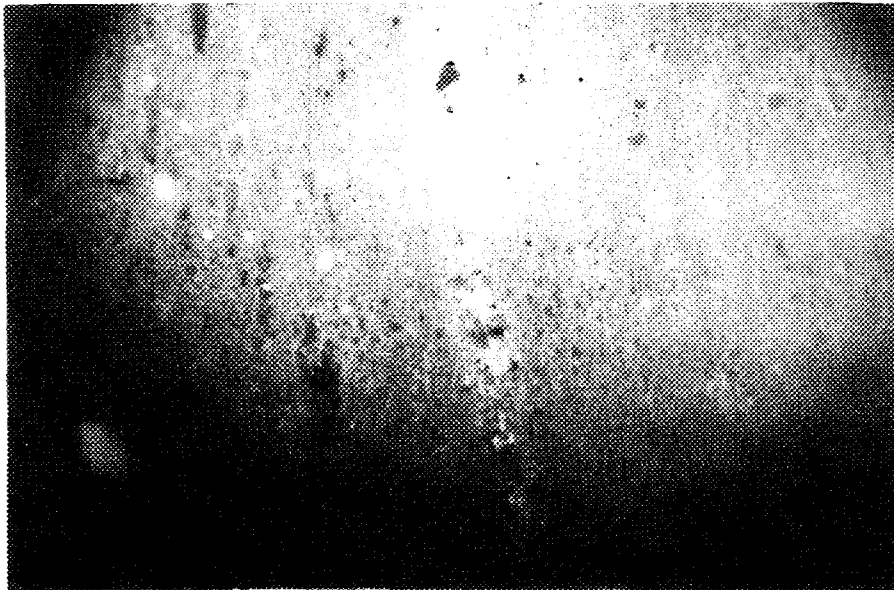


Fig. 4.6. Photomicrograph of organic-rich laminae of the Green River Formation. These laminae are not revealed in white light (reflected blue light at 250X).

sample population of at least 10 and no more than 25 measurements. Because of sample combustion, measurements were not taken for the Chattanooga and Green River Formation shales at 500 and 600°C, or the Alum Shale samples heated to 400°C and above. Included with the vitrinite measurements of the Chattanooga Shale and the Green River Formation are those of the vitrinite like organic material in the Alum Shale. Similar terminology has been employed for studies of other Cambrian shales (Glikson, Gibson, and Philp 1985), and it is clear that this Alum Shale maceral is not the true vitrinite of post-Silurian shales and coals. For the purposes of this study, however, the maceral properties were monitored as a function of thermal treatment as though they were true vitrinites.

The results from the reflectance analysis are presented in Table 4.2 and Fig. 4.7. It is clear that vitrinite reflectance increases systematically with increasing temperature and that the vitrinite in the Chattanooga Shale and Green River Formation behave similarly during thermal treatment. The untreated samples of Chattanooga and Green River Formation shales are of the same rank and remain the same throughout the incremental heating. Further, the maturation paths, as revealed by petrographic techniques, of these two notable shales have not been clearly defined in the literature; and it is interesting to note that the vitrinite of the Paleozoic Chattanooga Shale and the Cenozoic Green River Formation shales behaves similarly during thermal treatment despite obvious differences in the precursor plants of the vitrinite. The vitrinite from the more primitive land plants behave similarly to the vitrinite from the more evolved vascular plants. Reflectance values for the Alum Shale suggest a lower level of maturity for the untreated sample and for each heat-treated sample. The deviation about the mean is generally near 0.1% reflectance and is best for the Alum Shale. This level of precision is considered quite good for sedimentary organic material.

Table 4.2. Mean random vitrinite reflectances for shales that did not combust during heat treatment. Values for the Alum Shale are for the vitrinite like maceral

Temperature (°C)	Chattanooga Shale ^a	Green River Formation	Alum Shale
ambient	0.69 (0.13)	0.69 (0.11)	0.41 (0.04)
100	0.78 (0.10)	0.75 (0.11)	0.45 (0.03)
200	0.91 (0.07)	0.93 (0.10)	0.62 (0.08)
300	1.29 (0.12)	1.23 (0.12)	1.07 (0.13)
400	1.72 (0.03)	1.75 (0.03)	

^aStandard deviations (percent) are in parentheses. Given the dearth of vitrinite in most samples, no more than 25 and no fewer than 10 measurements were taken per sample.

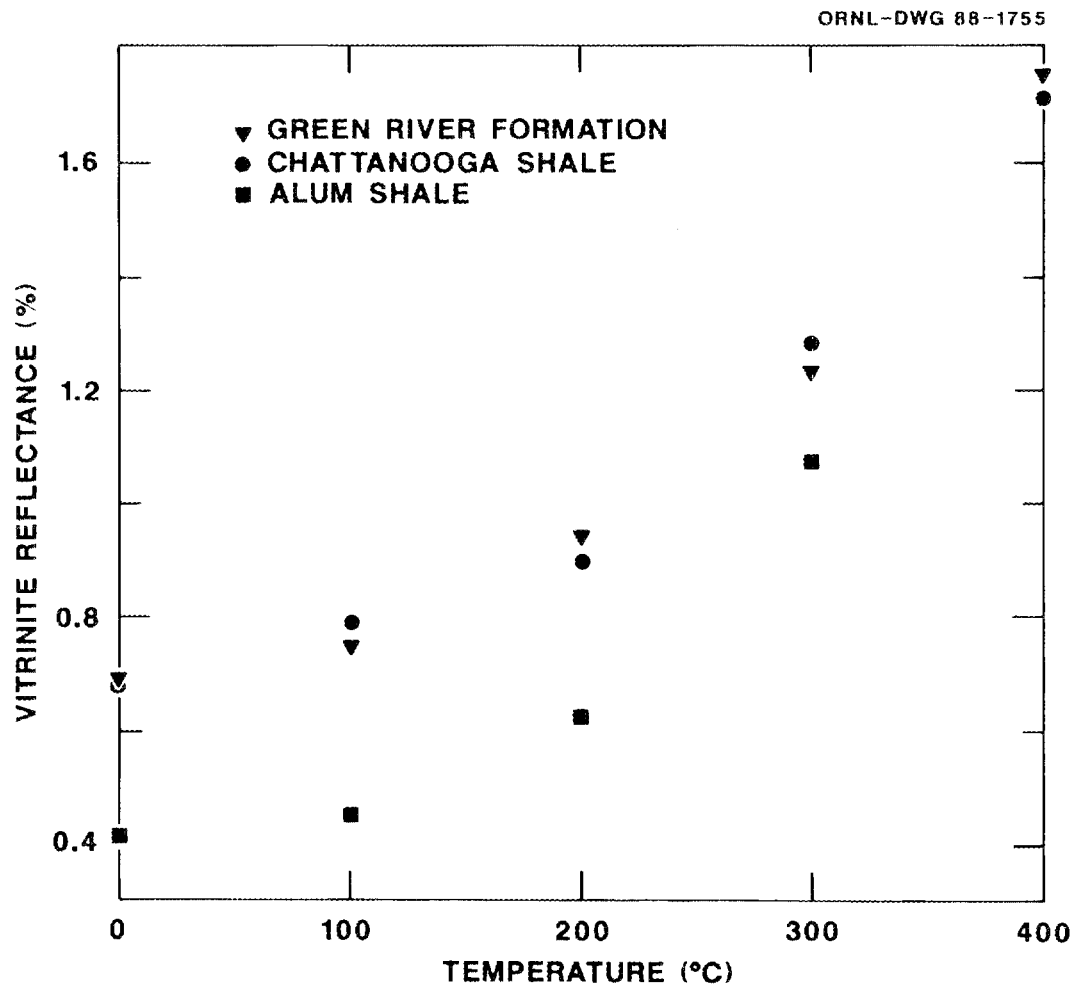


Fig. 4.7. Variation of mean random vitrinite like (Alum Shale) and vitrinite (Green River Formation and Chattanooga Shale) reflectance as a function of increasing temperature of heat treatment.

4.2.3 Quantitative Fluorescence Analysis

The fluorescence properties of each shale vary uniquely with increasing temperature and vitrinite reflectance. Fluorescence of the alginite from the Chattanooga Shale gradually shifts to the longer wavelengths from the yellow to the orange and decreases in fluorescence intensity (Fig. 4.8 and Table 4.3). At 300°C, the shift to the red becomes less subtle as some of the alginite spectra yield peaks in the orange (626 nm) wavelengths (Fig. 4.9). At 400°C the faint orange fluorescence can no longer be detected. This shift to the orange wavelengths at 300°C correlates well with a broad exothermic DTA peak from 340 to 480°C.

The fluorescence properties of the Alum Shale indicate that the organic matter is more sensitive to thermal effects than the kerogen in the Chattanooga Shale. Fluorescence is detected through 200°C, but measurable only in the initial and 100°C sample (Table 4.3), and may be characterized as weak to moderate yellowish-orange.

Measurable fluorescence is only slightly more persistent in the Green River Formation. The fluorescing macerals offer measurable intensities through 200°C but fade beyond detection at 300°C and above. The moderately intense orange bodies shift to the yellowish-orange in the 100 and 200°C samples, and there is some evidence that the spectra shift back to the longer wavelengths after heating to 200°C (Table 4.3).

The conspicuous fluorescence of these three shales varies uniquely upon thermal treatment. Measurable fluorescence of Chattanooga Shale alginite persists through 300°C, varies systematically over this temperature range, and may be correlated with DTA data. The fluorescence of Green River Formation kerogen is not measurable in the 300°C sample and might shift to the shorter wavelengths with increasing temperature. Alum Shale alginite and bituminite are most sensitive to thermal treatment, as measurable fluorescence intensities are observed only for samples heated to 100°C or not at all. Alum Shale fluorescence intensity increases with

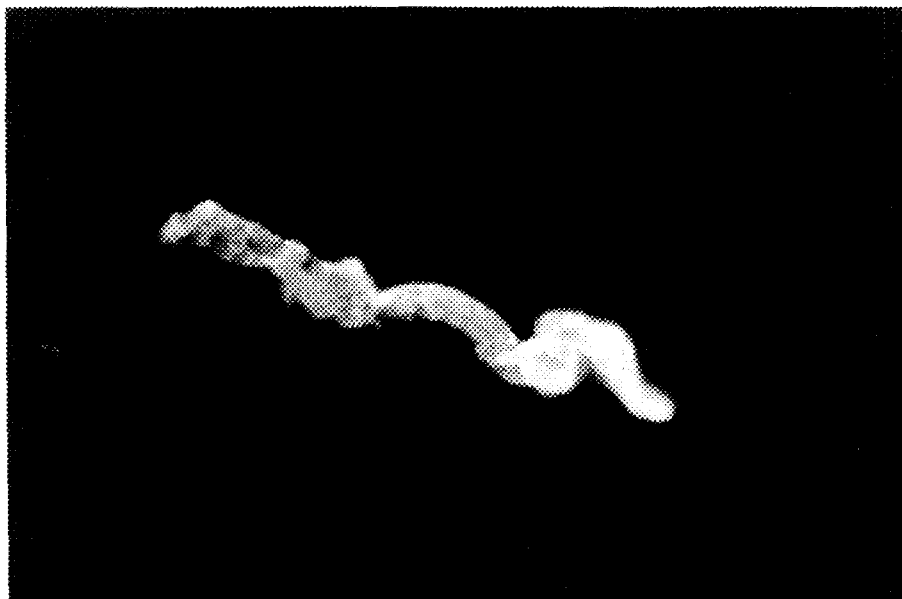


Fig. 4.8. Photomicrograph of yellow-orange alginite in Chattanooga Shale heat treated to 300°C (reflected blue light at 750X).

Table 4.3. Average fluorescence parameters for the Chattanooga Shale (alginite), Green River Formation (fluorescent fillings), and the Alum Shale (alginite)

Sample, heat treatment	Peak ^a (nm)	Q ^b	Q _{max} ^c
Chattanooga, untreated	572 (8) ^d	1.03 (0.10)	1.45 (0.08)
Chattanooga, 100°C	576 (5)	1.05 (0.12)	1.40 (0.08)
Chattanooga, 200°C	584 (2)	1.30 (0.08)	1.67 (0.08)
Chattanooga, 300°C	583 (5)	1.55 (0.08)	1.74 (0.06)
Chattanooga, 300°C	626 (1)	2.07 (0.10)	2.16 (0.10)
Green River Formation, untreated	610 (11)	1.70 (0.09)	1.82 (0.05)
Green River Formation, 100°C	584 (4)	1.16 (0.08)	1.36 (0.05)
Green river Formation, 200°C	589 (5)	1.38 (0.07)	1.63 (0.06)
Alum, untreated	585 (1)	1.65 (0.09)	1.90 (0.04)
Alum, 100°C	584 (1)	1.64 (0.04)	1.86 (0.04)

^aPeak (nm) is the wavelength of maximum intensity.

^bQ is the spectral quotient of the intensity at 650 nm divided by the intensity at 500 nm.

^cQ_{max} is the quotient of the intensity at the maximum wavelength divided by the intensity at 500 nm.

^dStandard deviations (percent) are given in parentheses.

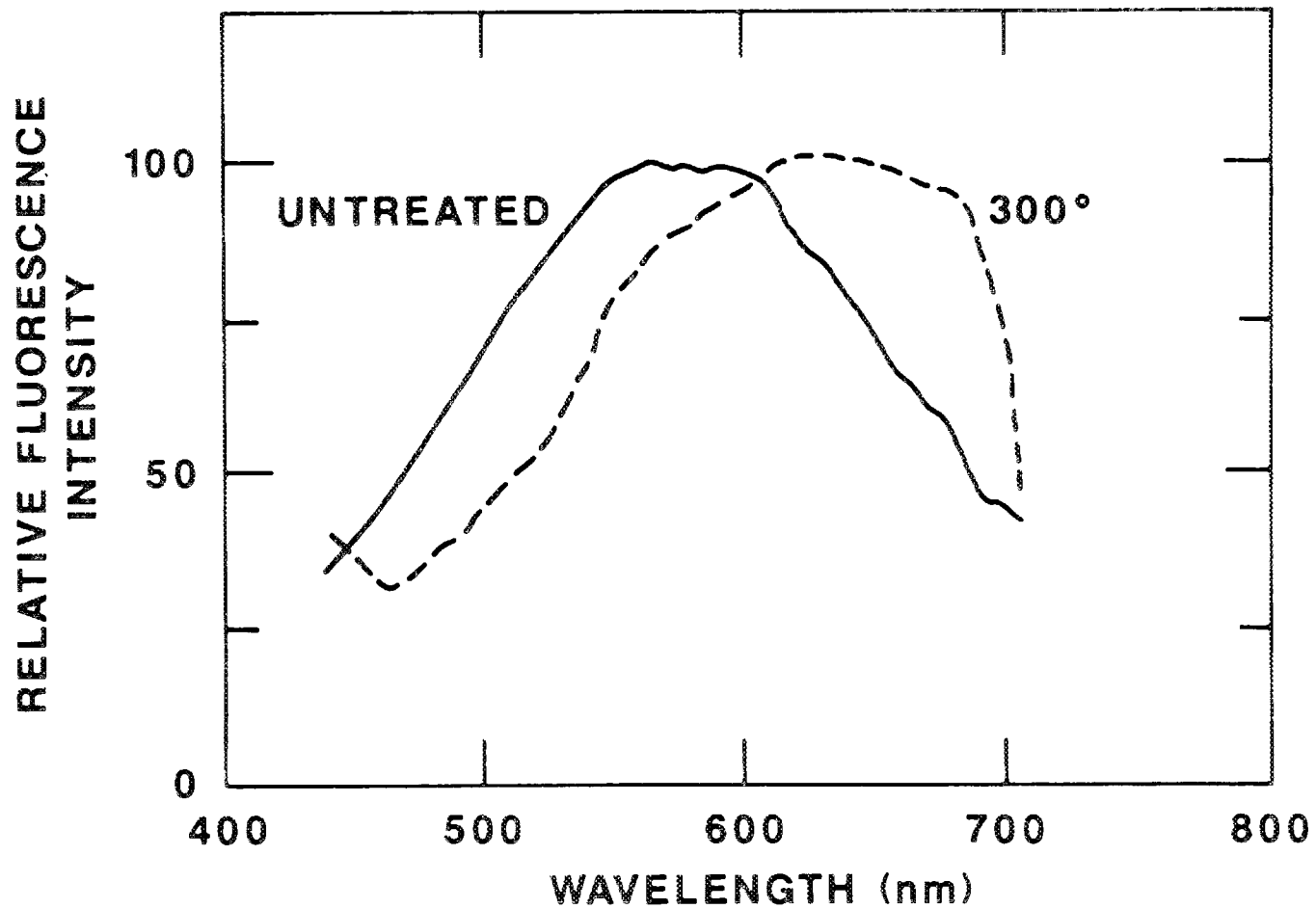


Fig. 4.9. Fluorescence spectra of untreated and heat-treated (300°C) alginite from the Chattanooga Shale showing the shift to longer wavelengths as a function of thermal treatment.

continued uv irradiation (i.e., positive alteration) in a manner described previously by Teichmüller and Wolf (1977).

4.2.4 Temporal Fluorescence Analysis

The alginite in the Chattanooga Shale samples heated up to and including 300°C and in the untreated Alum Shale samples offered enough fluorescence intensity to allow measurements of their fluorescence decays. On the assumption that these organic substances represent a molecular structure with a considerable fraction as a "mobile" phase consisting of smaller molecules, the fluorescence lifetime distribution recovery technique was used for these macerals. A plot of lifetimes (in nanoseconds) vs percentages is yielded. Thus, the amount of each user-selected lifetime is produced from each decay curve and permits the analysis of more than two or three lifetimes commonly yielded from the reiterative deconvolution technique.

Figure 4.10 is a collection of lifetime distributions for alginites from the Chattanooga Shale heated from ambient to 300°C. It is clear that the alginite from the samples heated to the highest temperatures yields distributions of almost exclusively subnanosecond components, unlike the untreated samples and those heated to 100°C, which show a wider distribution of fluorescence lifetimes with smaller subnanosecond percentages. The distributions from the untreated alginite of the Alum Shale more closely resemble the most thermally altered alginite of the Chattanooga Shale (Fig. 4.11). This behavior may result from differences in the algal components of the two shales or from the fact that the rank indicators of the Alum Shale yield suppressed values. This result is not surprising in liptinite-rich shales. That lifetime distributions of alginite fluorescence can be recovered and vary as a function of increasing temperature and vitrinite reflectance, however, are new and surprising results.

4.3 DISCUSSION

The fluorescence properties of whole-rock mounts of thermally altered Alum Shale, Chattanooga Shale, and Green River Formation shale

ORNL-DWG 88-1757

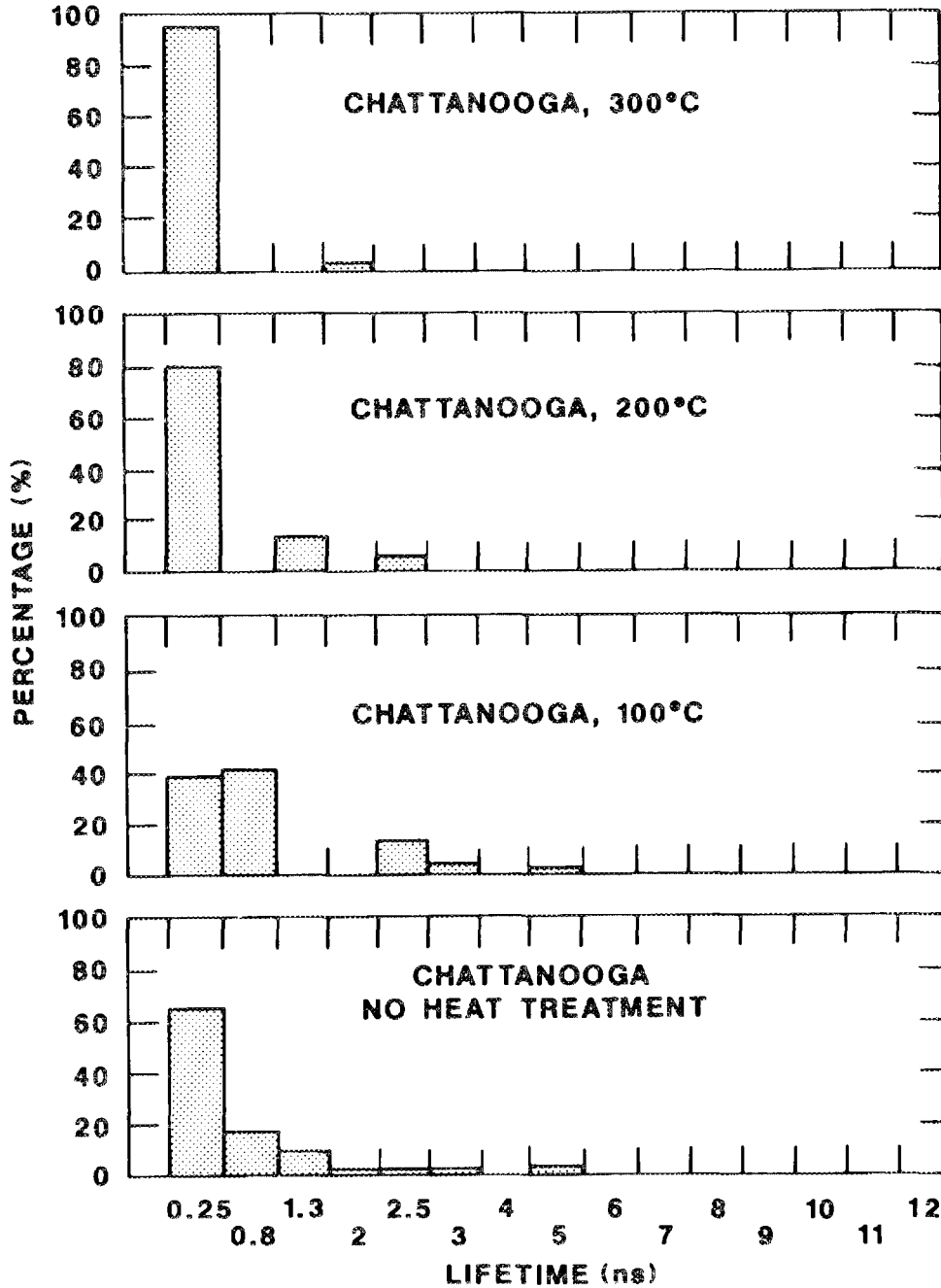


Fig. 4.10. Fluorescence lifetime distributions of Chattanooga Shale as a function of thermal treatment. Note the progressive increase in subnanosecond components with increasing temperature of heat treatment.

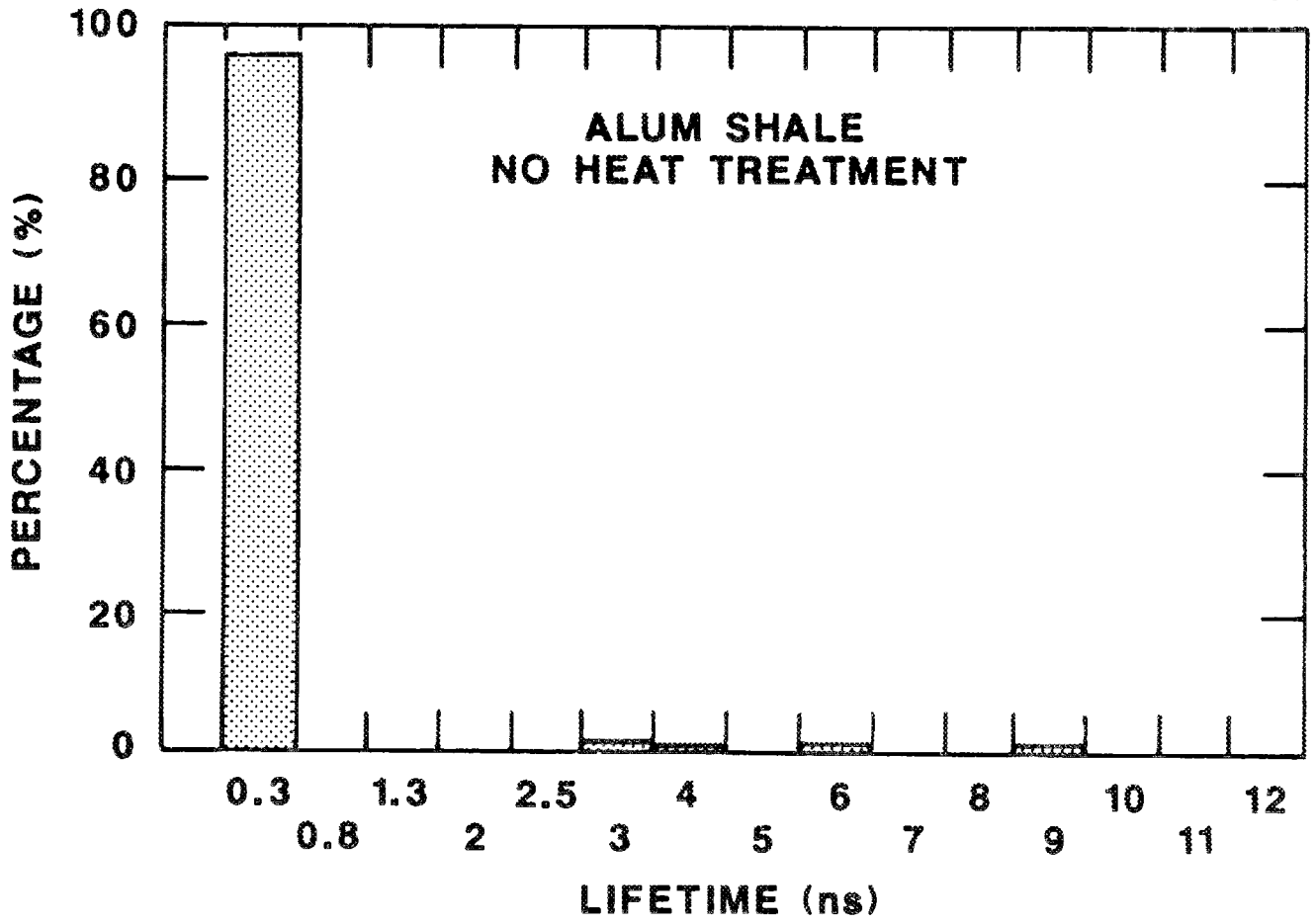


Fig. 4.11. Fluorescence lifetime distribution of untreated Alum Shale alginite clearly showing the high percentage of the sub-nanosecond component.

were studied petrographically using white- and blue-light techniques. Each of these shales possesses a unique maceral assemblage that is better studied using a combined maceral analysis. More liptinites are counted in blue light, where the contrast between the maceral and the mineral matrix is greatest. For example, liptinites in laminae from the Green River Formation are easily revealed by their fluorescence properties. Similarly, the strong yellow fluorescence of the alginites of the Chattanooga Shale contrasts sharply with the largely nonfluorescent mineral matrix.

Changes as a function of thermal treatment can also be monitored petrographically. Vitrinite reflectance varies systematically and uniquely for these shales. Consequently, these early results indicate that vitrinite reflectance may be used as a thermometer of rapid thermal alteration, much like its use with coals and petroleum source rocks. In this case, the Chattanooga and Green River Formation shales follow similar maturation paths, despite their age and compositional differences. Alginite spectra also vary systematically with increasing temperature, recording a shift to the longer wavelengths from the yellow to the orange (561 to 626 nm). The shift to the orange wavelengths at 300°C correlates well with a broad exothermic DTA peak from roughly 340 to 480°C. Temporal analyses indicate fluorescence lifetime distributions heavily favoring subnanosecond components, particularly as temperature and rank increase. For the Chattanooga Shale alginites, nanosecond and subnanosecond fluorescence lifetimes are recovered at low thermal treatment temperatures. However, as the temperature of heat treatment increases, the distribution clearly favors the shorter, subnanosecond lifetimes.

The techniques employed in this portion of the study demonstrate the potential utility of microfluorometry in describing the behavior of organic matter in shales under a variety of conditions. It would be especially interesting to combine these techniques with autoradiography to investigate which organic phases may be most reactive to particular radioelements. The alteration of kerogen during hydrothermal reaction could also be characterized and yield insight into the degradation of

kerogen and the formation of potential organic complexants. Further quantification and refinement of these techniques will be necessary to advance such studies. One aspect of this refinement is discussed in the next section.

5. TIME-RESOLVED FLUORESCENCE SPECTRA OF STANDARD ORGANIC COMPOUNDS

Fluorescence is the type of luminescence that describes the emission of a photon induced by the return of an excited electron to the ground state. Excited states are short-lived and may either revert back to the ground state or undergo a chemical change to form a new species. A list of possible photochemical processes includes

1. vibrational relaxation,
2. fluorescence,
3. intersystem crossing,
4. internal conversion,
5. phosphorescence,
6. energy transfer,
7. photochemical reaction, and
8. radiationless decay (Allen and McKellar 1980).

Substances that exhibit fluorescence are called fluorophores and generally possess delocalized electrons in double bonds (i.e., sp^2 , sp hybridized states). It is the p-orbital electron that is generally assumed to be excited by incident near-uv light. Thus, fluorescence microscopy is a promising tool for the study of those organic compounds containing π -molecular bonds that are able to absorb uv light.

It is widely assumed that organic matter in coals is cross-linked macromolecular structures (Green et al. 1982). Similarly, the organic matter in sedimentary rocks may be considered as macromolecules. The macromolecular theory, as proposed by Green et al. (1982), and Davidson (1982) describes a cross-linked macromolecule consisting of hydroaromatics and aromatics bridged by aliphatics and ethers. These investigators further describe a relatively minor but important group of smaller molecules trapped within the larger structure. Little is known regarding the chemistry of these smaller, "mobile-phase" molecules. Thus, the objective of this study was to characterize the spectral and temporal fluorescence properties of several low-molecular-

weight organic compounds that may occur as mobile-phase molecules in sedimentary rocks and that could be studied in the future through solvent-extraction and in situ photochemical analyses.

5.1 METHODS

The techniques used in this study include fluorescence microscopy, in both the spectral and temporal domains, and absorption spectroscopy. Absorption spectroscopy was initiated because many of the organic compounds do not fluoresce. Absorption spectra were obtained from a Lambda 5 uv/VIS spectrophotometer with an excitation beam in the uv range (332.8 nm), with water as an absorption standard. Absorption was measured as a function of wavelength from 330.0 to 450.0 nm.

The laser fluorescence microscopy system is shown in Fig. 5.1. The conventional fluorescence spectra were obtained with continuous-wave (cw) illumination (100-W Hg lamp) of the particular compound in a nonfluorescent quartz cuvette. A tungsten bulb was used to determine the spectral response of the system by the following relationship:

$$T_T = \frac{T_m}{E_m} \cdot E_T \quad ,$$

where

T_T is the corrected tungsten bulb spectrum,

T_m is the measured or raw spectrum,

E_m is the measured or raw standard lamp spectrum,

E_T is the known standard lamp spectrum. The determination of the spectral response for any given microscope configuration is completed using the relationship:

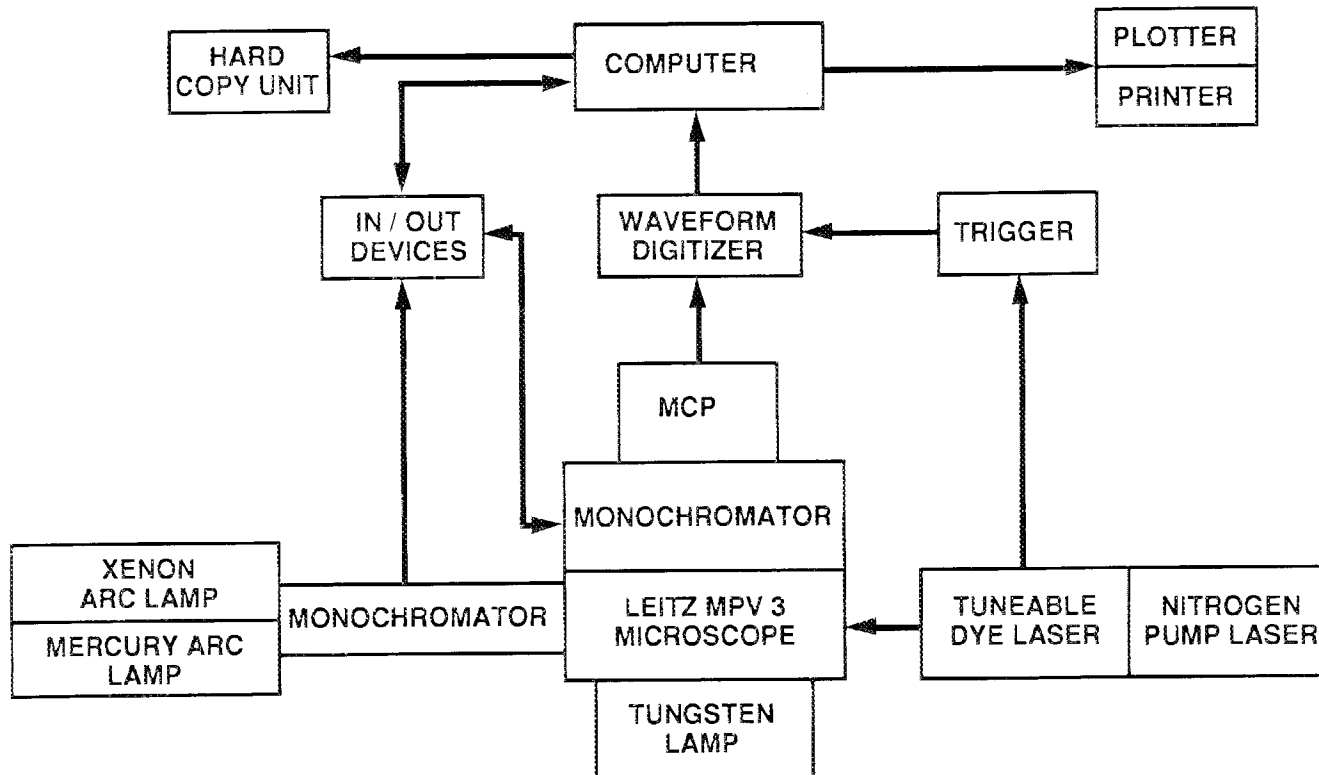


Fig. 5.1. Schematic diagram of laser fluorescence system showing the input Hg bulb (left) and nitrogen-pumped tunable-dye laser (right). Emission is detected by a microchannel plate (MCP) and sent to a computer.

$$S(\lambda) = \frac{T_m(\lambda)}{T_T(\lambda)} ,$$

where $S(\lambda)$ is the response at a given wavelength of emission. Finally, the corrected fluorescence spectrum is expressed as

$$R(\lambda) = \frac{R_m(\lambda)}{S(\lambda)} ,$$

where $R_m(\lambda)$ is the raw, or uncorrected, fluorescence spectrum. It is this process that yields the spectral properties of fluorescing substances.

Obtaining the temporal properties (i.e., characteristic fluorescence lifetimes and percentages) is not as transparent and is only now becoming a viable tool for the examination of fluorescing compounds. Two techniques described in Landis et al. (1987) and James et al. (1987) can be employed for the recovery of characteristic temporal data from fluorescence decay: (1) The iterative reconvolution technique and least-squares fitting of Landis et al. (1987) permits the deconvolution of decays containing up to three components and were used in this study. This method assumes noninteracting fluorophores. (2) The recovery of underlying lifetime distributions from fluorescence decays permits more than three lifetimes to be examined and requires no prior knowledge of the underlying distribution (James et al. 1987). Both techniques are relatively new, have not been routinely applied to the geosciences, and have some limitations to their applications. Iterative reconvolution requires a prior knowledge of the underlying lifetime distributions, which is not generally available for coals and dispersed sedimentary organic matter. It is also not useful for

mixtures of more than three components. The distribution technique does not immediately yield the precise lifetimes and still requires better fitting functions (James et al. 1987). In this study, several examples of each technique are presented for the various fluorescing compounds, with full knowledge of the limitations in mind.

5.2 RESULTS

Organic compounds (Table 5.1) were chosen for study to represent the major classes of compounds with unique characteristics. These organic compounds are low-molecular-weight analogs to more complex compounds found in sedimentary organic matter. The fluorescence behavior of these analogs should represent that of the functional groups found in the more complex natural organics. More detailed studies in the future will emphasize organic compounds that are more closely representative of natural organic matter found in sedimentary rocks. The fact that most of these simple organic compounds do not fluoresce was confirmed by visual inspection and the absorption analysis (Table 5.1). Strongly fluorescent compounds such as the aromatics yielded absorption spectra that exceeded all user-definable absorption limits on the spectrophotometer. It is not surprising that the alkanes do not fluoresce, given their saturated molecular bonding structure (sp^3). Further, laboratory observation indicates that those samples with an absorbance of <0.70 mAU usually did not offer sufficient intensity for detection on this particular system. It is easy to see that the alkenes, most of the alkynes and carboxylic acids, and many of the other compounds do not absorb uv light well. Several compounds that absorb uv light modestly might well offer suitable intensities on other, more sensitive systems. On the other hand, the heteroatom pyrrole, with one less carbon than pyridine, absorbs quite well. Such is the case for quinoline as well.

Table 5.2 is a listing of the fluorescence properties of these compounds. Straight-chain compounds (octyne and fatty acids) and the nitrogen compounds (aromatics and heteroatom) exhibit blue fluorescence. As a general rule, the nitrogen compounds exhibit weaker

Table 5.1. Listing of absorbances of the compounds included in this study

Compound	Absorbance (mA)
pentane	a
hexane	a
heptane	0.0010
octane	0.0025
nonane	0.0013
decane	0.0423
pentene	0.0350
hexene	a
heptene	0.0070
octene	0.0255
nonene	0.1160
decene	0.0030
pentyne	a
hexyne	0.0630
heptyne	0.0480
octyne	0.7000
nonyne	0.5400
heptanoic acid	a
octanoic acid	0.7800
nonanoic acid	0.1200
decanoic acid	0.6800
pyrrole	1.0860
pyridine	0.3700
quinoline	5.0000 ^b
acridine	5.0000 ^b
isoprene	0.0069
pristane	0.0450
water	0.0000

^anot detected.

^bMaximum absorbance value.

Table 5.2. Spectral and temporal properties of the fluorescing compounds

Compound	^a Spectral properties			^b Temporal properties					
	PEAK (nm)	Q	Q _{max}	T1(ns)	T2(ns)	T3(ns)	P1(%)	P2(%)	P3(%)
Octyne	449	0.11	2.31	6.86	2.10	0.44	49.0	28.7	22.3
Octanoic Acid	437	0.00	1.85	0.67	5.34		38.3	61.7	
Decanoic Acid	438	0.00	5.11						
Nonanoic Acid	439	0.05	2.87						
Pyrrole	440	0.00	2.82	3.04	0.48		60.6	39.4	
Pyridine	439	0.19	3.14						
Quinoline	439	0.59	1.74	0.38	3.91		43.6	56.4	
Acridine	429	0.00	10.25	10.40	0.40		10.2	89.8	
Thiophene	549	0.99	3.52						
Anthracene	403	0.00	330.13	4.11	0.32		97.0	3.0	
Tetracene	478	0.24	1.4	5.49	2.06		93.3	6.7	
Pentacene	580	1.79	3.08	1.62	2.70	11.62	25.8	16.9	53.3

^aPeak (nm) is the spectral maximum, wavelength of maximum intensity; Q is the spectral quotient, ratio of intensity at 650 nm to the intensity at 500 nm; and Q_{max} is the ratio of maximum intensity to intensity at 500 nm.

^bT_{1,2,3} are characteristic decay lifetimes (ns); and P_{1,2,3} are percentages of characteristic lifetimes in the spectra.

fluorescence intensities than octyne and octanoic acid. For all of these compounds except acridine, the nanosecond lifetimes dominate; but the subnanosecond lifetimes contribute significantly to the decay. Figure 5.2 shows the emission spectrum and fluorescence decay of octyne. These are typical data acquired from our analyses, and clearly the emission spectrum is a composite of several fluorophores resolved from the characteristic fluorescence decay.

Excellent results were obtained from the linearly fused aromatics. Each additional ring in the structure is accompanied by a spectral shift to the longer visible wavelengths and longer lifetimes (Fig. 5.3 and Table 5.2). Spectrally, these aromatics shift from strong blue fluorescence (anthracene) to weak yellowish-orange (pentacene); and although the resolution of similar lifetimes remains a topic of further research, fluorescing compounds with different lifetimes can be fingerprinted in a noninteracting mixture (Fig. 5.4). In this case, the fluorescence decay of anthracene, POPOP [p-bis(2-(5-Phenyloxazolyl))], and an anthracene-POPOP mixture was acquired over a spectral range of 390 to 470 nm in 10-nm increments. It is clear that the pulsed-integrated spectrum of the mixture is a composite of the anthracene and POPOP spectra. Further, the resolved lifetimes of the mixture compare well with the acquired lifetimes of the individual liquids. Thus, for noninteracting liquid mixtures, this technique shows promise as an extension of conventional fluorescence spectral analysis, in which the contributing fluorophores are lost in the composite spectrum.

5.3 DISCUSSION

A Leitz MPV III Orthoplan microscope, interfaced on the input end with a 100-W Hg-arc lamp and nitrogen-pumped, tunable-dye laser, was used for both cw and pulsed-laser, near-uv (365 and 395 nm, respectively) excitation of a group of standard organic compounds. Resultant data extracted from the emission spectra are the spectral maximum and quotient. Temporal data from the analyzed decay curves include percentage contributions, fluorescence lifetimes (nanosecond

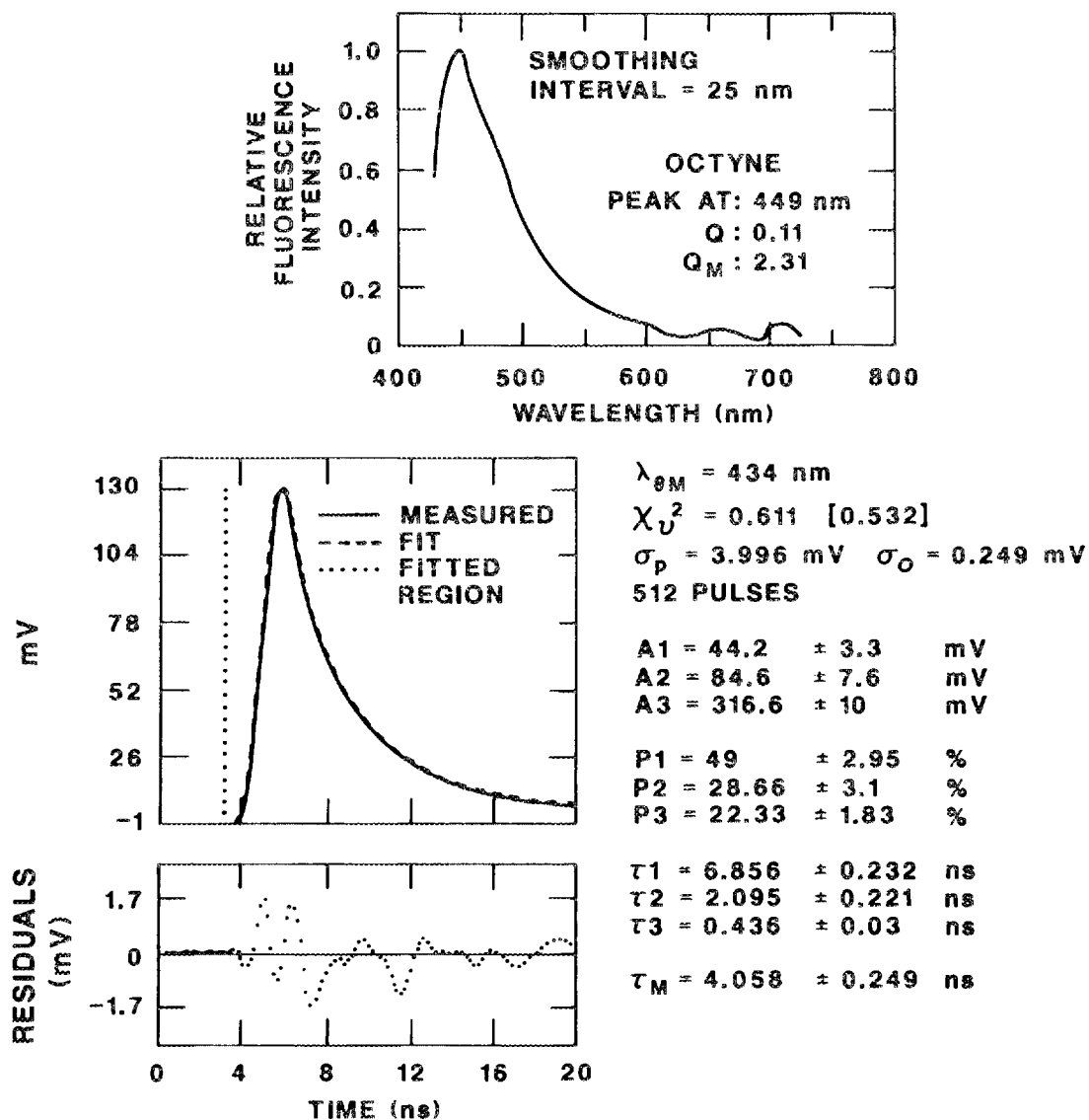


Fig. 5.2 Graphical output of spectral (top) and temporal (bottom) fluorescence analyses. At the top, octyne emission expresses blue fluorescence. The smoothing interval was 25 nm. At the bottom, the acquired and fitted decays (overlapping) are presented as intensity (mV) versus time (ns) plots. Characteristic lifetimes, distributions, and intensities are included in the table to the right. Results are based on 512 pulses and an emission wavelength of 434 nm.

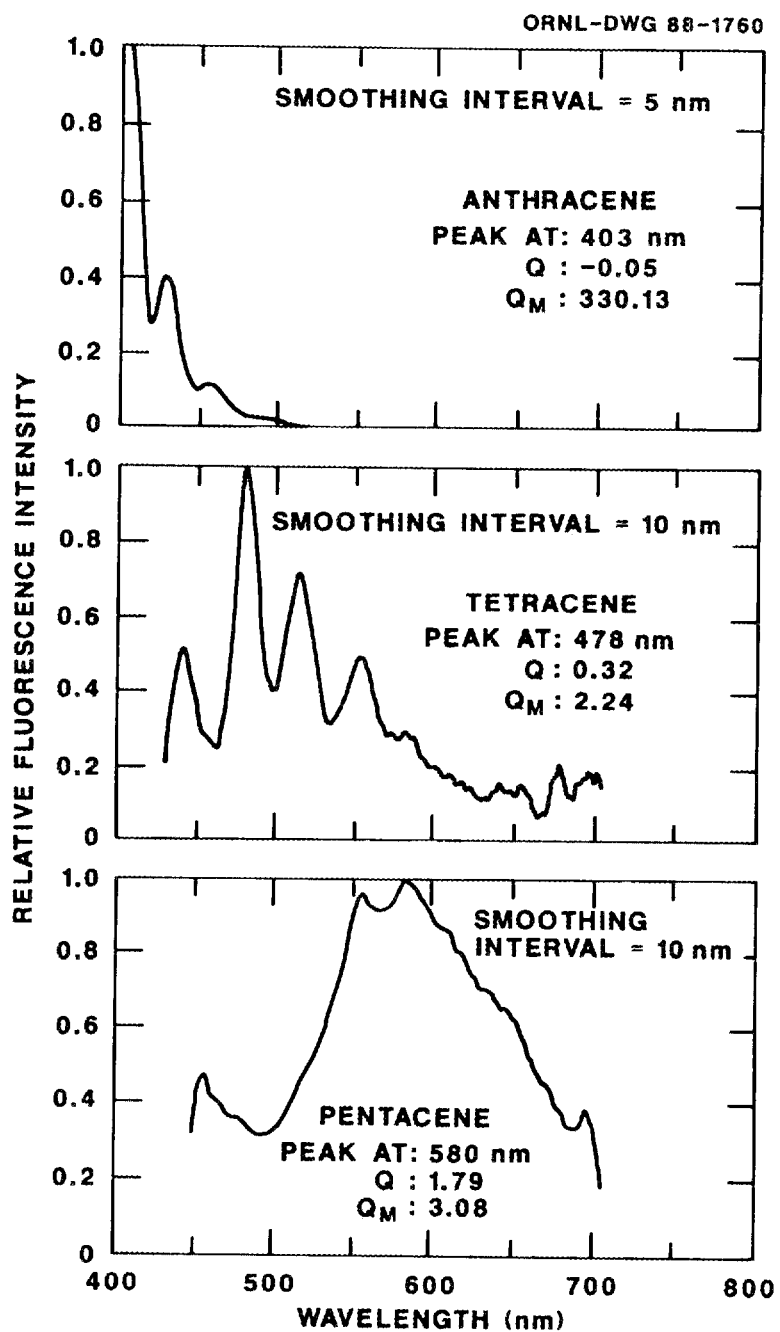


Fig. 5.3. Spectral shift of linearly fused aromatics. At the top, anthracene records a strong blue fluorescence. At the bottom, pentacene records a yellowish-orange emission.

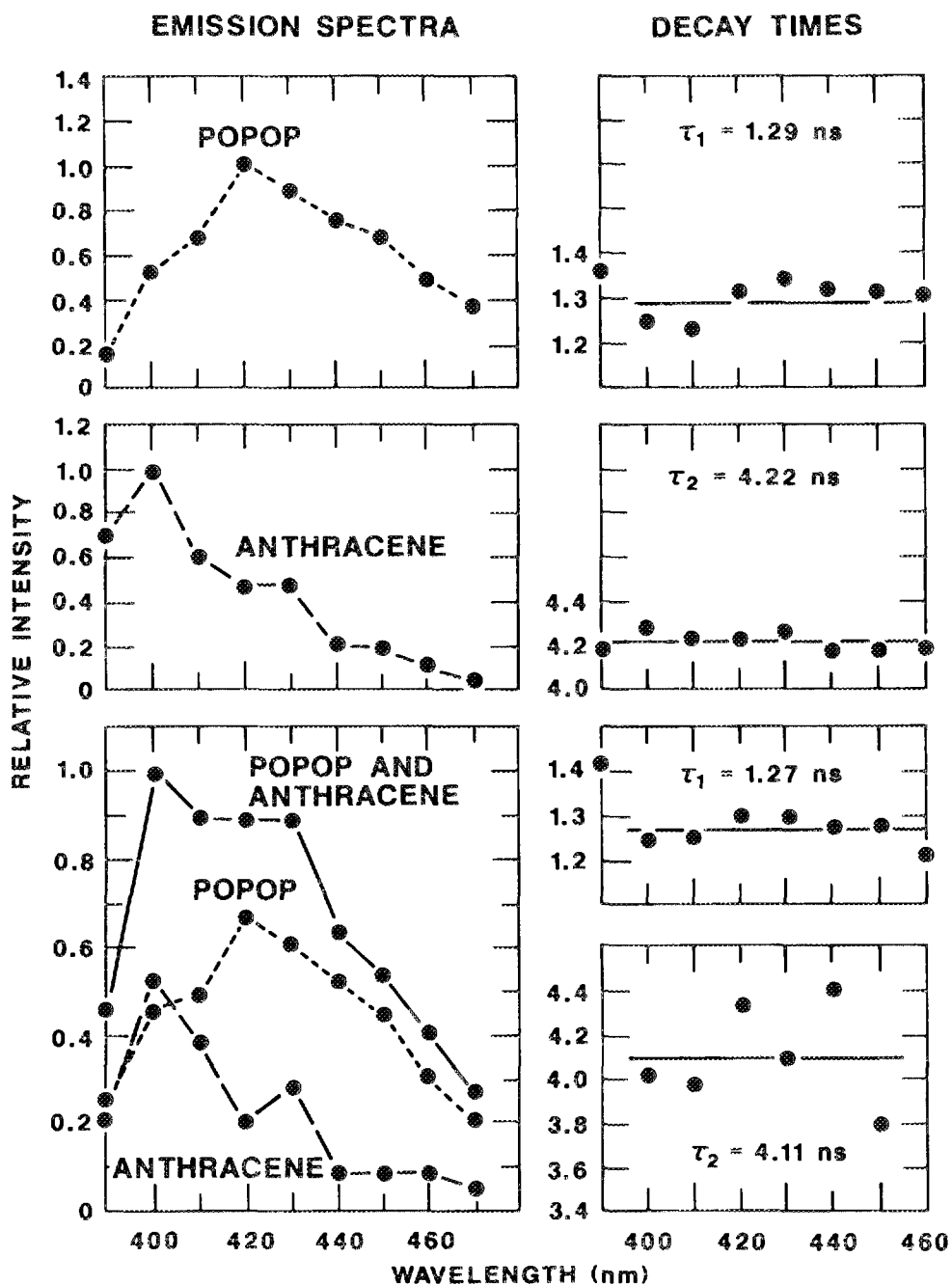


Fig. 5.4. Time-resolved data of fluorescence decay times and emission intensity over the spectral range of 390 to 470 nm for anthracene, POPOP, and a mixture of the two. Borst, W. L., S. Gangopadhyay, and M. W. Pleil. 1987. Fast analog technique for determining fluorescence lifetimes of multicomponent materials by pulsed laser. SPIE, - The Int. Soc. for Opt. Eng. Proc. 43:15-23.

and subnanosecond), and Einstein A-coefficients (intensity coefficient). These temporal data are acquired from iterative reconvolution or recovered as a distribution of user-defined lifetimes. In either case, characteristic lifetimes for each fluorescing compound are recovered.

The group of organic compounds studied included the alkanes, alkenes, alkynes, carboxylic acids, heteroatoms, and several linearly fused aromatics. Alkanes do not fluoresce and most of the other compounds that contain π -bonds were also observed not to fluoresce. Indeed, they did not absorb uv light (333 nm). Nonaromatic compounds fluoresce strongest in the blue wavelengths. Linearly fused aromatics display a shift to the longer wavelengths and decrease in fluorescence intensity as each additional ring is added to the structure. The fluorescence lifetimes of these compounds are dominantly in the nanosecond range, with subnanosecond lifetimes contributing less to the total emission. Thus, despite current limitations, time-resolved fluorescence microscopy is a viable technique worthy of continued developmental research.

The identification and estimation of specific organic compounds in sedimentary rocks would be a significant advancement. To accomplish this advancement, further research is needed in the following areas: (1) the analysis of additional individual compounds that may be common to organic matter in sedimentary rocks, (2) the investigation of dilution affects on the fluorescence characteristics, (3) further studies on the mixtures of organic compounds, and (4) the characterization of fluorescence spectra of organic compounds in a variety of mineral matrices.

6. REFERENCES

- Allen, N. S., and J. F. McKellar. 1980. Photochemistry of Dyed and Pigmented Polymers. Applied Science Publishers, London.
- Andersson, A., B. Dahlman, D. G. Gee, and S. Snäll. 1985. The Scandinavian shales. Avhandlingar Och Uppsatser I A4. Series Ca, NR 56. Swedish Geological Survey, Stockholm, Sweden.
- Bell, R. T. 1978. Uranium in black shales: A review. pp. 307-329. IN: M. M. Kimberly (ed.), Uranium deposits: Their mineralogy and origin Vol. 3. Mineralogical Association of Canada Short Course, Toronto, Canada.
- Bertrand, P., J-L. Pitton, and C. Bernaud. 1986. Fluorescence of sedimentary organic matter in relation to its chemical composition. Org. Geochem. 10:641-647.
- Crelling, J. C. 1983. Current uses of fluorescence microscopy in coal petrology. J. Microscopy. 132:251-266.
- Croff, A. G., T. F. Lomenick, R. S. Lowrie, and S. H. Stow. 1986. Evaluation of five sedimentary rocks other than salt for geologic repository siting. ORNL-6241.
- Davidson, R. M. 1982. Coal Science, Vol. 1. IN: J. W. Larons, M. L. Gorbaty, and I. Wender (eds.), Academic Press, New York.
- Drummond, S. E. and D. A. Palmer. 1986. Thermal decarboxylation of acetate. Part II. Boundary conditions for the role of acetate in the primary migration of natural gas and the transportation of metals in hydrothermal solutions. Geochim. Cosmochim. Acta. 50:825-834.
- Eglinton, T. I., S. J. Rowland, C. D. Curtis, and A. G. Douglas. 1985. Kerogen-mineral reactions at raised temperatures in the presence of water. Org. Geochem. 10:1041-1052.
- Fisher, J. B. 1987. Distribution and occurrence of aliphatic acid anions in deep subsurface waters. Geochim. Cosmochim. Acta. 51:2459-2468.

- Glikson, M., D. L. Gibson, and R. P. Philp. 1985. Organic matter in Austrian Cambrian oil shales and other Lower Paleozoic shales. *Chem. Geol.* 51:175-191.
- Green, T., J. Kovac, D. Brenner, and J. W. Larsen. 1982. Coal structure. IN: R. A. Meyers (ed.), Academic Press, New York.
- Huizinga, B. J., E. Tannenbaum, and I. Kaplan. 1987. The role of minerals in the thermal alteration of organic matter - IV. Generation of n-alkanes, acyclic isoprenoids, and alkenes in laboratory experiments, *Geochim. Cosmochim. Acta.* 51:1083-1097.
- James, D. R., Y-S. Liu, N. O. Petersen, A. Siemiarczuk, B. D. Wagner, and W. R. Ware. 1987. Recovery of underlying distributions of lifetimes from fluorescence decay data, *Fluorescence Detection.* SPIE. 743:117-122.
- Kawamura, K. and I. Kaplan. 1987. Dicarboxylic acids generated by thermal alteration of kerogen and humic acids. *Geochim. Cosmochim. Acta.* 51:3201-3207.
- Khorasani, G. K. 1987. Novel development in fluorescence microscopy of complex organic mixtures: Application in petroleum geochemistry. *Org. Geochem.* 11:157-168.
- Landis, C. R. and J. C. Crelling. 1985. Changes in the fluorescence properties of selected Hartshorne seam coals with rank, *Intl. Conf. Coal Science*, Sydney, Australia.
- Landis, C. R., G. W. Sullivan, M. W. Pleil, W. L. Borst, and J. C. Crelling. 1987. Pulsed laser fluorescence microscopy of coal macerals and dispersed organic material, *Fuel* 66, 984-991.
- Lee, S. Y., L. K. Hyder, and P. D. Alley, 1988, Mineralogical characterization of selected shales in support of nuclear waste repository studies. ORNL/TM-10567.
- Lyons, P. C., D. M. Hercules, J. J. Morelli, G. A. Sellers, D. Mattern, C. L. Thompson-Rizer, F. W. Brown, and M. A. Millay. 1987. Application of laser microprobe (LAMMA 1000) to "fingerprinting" of coal constituents in bituminous coal. *Intl. J. Coal Geol.* 7:185-194.

- Martinez, L., B. Pradier, and P. Bertrand. 1987. The
microspectrofluorometry in organic petrology. C. R. Acad. Sci.
Paris. Series III. 304(9):441-446.
- McCarthy, J. T. and M. Teichmüller. 1972. Classification of coals
according to degree of coalification by reflectance of the
vitrinite component. Fuel 51:64-68.
- Ottenjann, K., M. Teichmüller, and M. Wolf. 1975. Spectral
fluorescence measurements of sporinites in reflected light and
their applicability for coalification studies. pp. 49-65. IN:
B. Alpern (ed.), Petrographie Organique et Potential Petrolier.
- Palmer, D. A. and S. E. Drummond. 1986. Thermal decarboxylation of
acetate. Part I. The kinetics and mechanism of reaction in aqueous
solution. Geochim. Cosmochim. Acta. 50:813-824.
- Smith, G. C. and A. C. Cook. 1980. Coalification paths of exinite,
vitrinite, and inertinite. Fuel. 59:641-646.
- Spackman, W. 1958. The maceral concept and the study of modern
environments as a means of understanding the nature of coal,
Trans. N.Y. Acad. Sci., Ser. II. 20(5):411-423.
- Spackman, W., A. Davis, and G. D. Mitchell. 1976. The fluorescence of
liptinite macerals, Brigham Young University Coal Studies.
22(Pt.3):59-75.
- Stopes, M. C. 1935. On the petrology of banded bituminous coals.
Fuel. 14:4-13.
- Teichmüller, M. 1974. Generation of petroleum-like substances in coal
seams as seen under the microscope. IN: B. Tissot, and F. Bienner
(eds.), Advances in organic geochemistry 1973. Editions Technip,
Paris, France.
- Teichmüller, M. 1986. Organic petrology of source rocks, history and
state of the art. Org. Geochem. 10:581-599.
- Teichmüller, M. and M. Wolf. 1977. Application of fluorescence
microscopy in coal and oil exploration. J. Microscopy.
109:49-73.

- Teichmüller, M. and B. Durand. 1983. Fluorescence microscopical rank studies on liptinites and vitrinites in peat and coals, and comparisons with results of the rock-eval pyrolysis. *Intl. J. Coal Geol.* 2:197-230.
- Thornton, E. C. and W. E. Seyfried. 1987. Reactivity of organic-rich sediment in seawater at 350°C, 500 bars: Experimental and theoretical constraints and implications for the Guaymas Basin hydrothermal system. *Geochim. Cosmochim. Acta.* 51:1997-2010.
- Von Damm, K. L. 1987. Geochemistry of shale groundwaters: Survey of available data and postulated mineralogic controls on composition. ORNL/TM-10488.
- Von Damm, K. L. 1988. A comparison of the Guaymas Basin hydrothermal solutions to other sedimented systems and experimental results. IN: AAPG Memoir: The Gulf and Peninsula Province of the Californias (submitted).
- Von Damm, K. L. and K. O. Johnson. 1987. Geochemistry of shale groundwaters: Results of preliminary laboratory leaching experiments. ORNL/TM-10535.

INTERNAL DISTRIBUTION

- | | | | |
|--------|------------------|--------|-----------------------------|
| 1. | W. D. Arnold | 21. | J. W. Ranney |
| 2. | T. Baer | 22. | D. E. Reichle |
| 3. | A. G. Croff | 23. | T. H. Row |
| 4. | M. P. Farrell | 24-25. | S. H. Stow |
| 5. | C. W. Gehrs | 26. | R. I. Van Hook |
| 6. | T. M. Gilliam | 27. | W. Van Winkle |
| 7. | S. G. Hildebrand | 28. | V. C. A. Vaughen |
| 8. | P. C. Ho | 29. | K. L. Von Damm |
| 9. | D. D. Huff | 30. | R. G. Wymer |
| 10-15. | G. K. Jacobs | 31. | Central Research Library |
| 16. | S. Y. Lee | 32-46. | ESD Library |
| 17. | T. F. Lomenick | 47-48. | Laboratory Records Dept. |
| 18. | R. E. Meyer | 49. | Laboratory Records, RC |
| 19. | M. E. Mitchell | 50. | ORNL Patent Office |
| 20. | M. L. Poutsma | 51. | ORNL Y-12 Technical Library |

EXTERNAL DISTRIBUTION

52. D. Alexander, DOE-Office of Civilian Radioactive Waste Management, 1000 Independence Ave., S.W., Washington, DC 20585
53. I. Alterman, DOE-Office of Civilian Radioactive Waste Management, 1000 Independence Ave., S.W., Washington, DC 20585
54. R. Baker, DOE-CHO, 9800 S. Cass Avenue, Chicago, IL 60439
55. S. J. Brocoum, DOE-Office of Civilian Radioactive Waste Management, 1000 Independence Ave., S.W., Washington, DC 20585
56. D. G. Brookins, 3410 Groman Ct., N.E. Albuquerque, NM 87110
57. R. Cady, DOE-Office of Civilian Radioactive Waste Management, 1000 Independence Ave., S.W., Washington, DC 20585
58. M. K. Cline, Roy F. Weston, Inc., 2301 Research Blvd., Rockville, MD 20850
59. R. R. Colwell, Director of Maryland Biotechnology Institute, University of Maryland, Rm. 2A, Elkins Building, College Park, MD 20742
60. W. E. Cooper, Department of Zoology, College of Natural Sciences, Michigan State University, East Lansing, MI 48824
61. N. H. Cutshall, 10461 White Granite Dr., Suite 204, Oakton, VA 22124
62. K. Cyscinski, Roy F. Weston, Inc., 2301 Research Blvd., Rockville, MD 20850
63. P. A. Domenico, Center for Tectonophysics, Texas A&M University, College Station, TX 77843

64. N. Eisenberg, DOE-Office of Civilian Radioactive Waste Management, 1000 Independence Ave., S.W., Washington, DC 20585
65. G. Faulkner, DOE-Office of Civilian Radioactive Waste Management, 1000 Independence Ave., S.W., Washington, DC 20585
66. A. Fossum, RE/SPEC, Inc., P. O. Box 725, Rapid City, SD 57701
67. M. Frie, DOE-Office of Civilian Radioactive Waste Management, 1000 Independence Ave., S.W., Washington, DC 20585
68. P. F. Gnirk, RE/SPEC, Inc., P. O. Box 725, Rapid City, SD 57701
69. S. Gonzales, Earth Resource Associates, Inc., 295 E. Dougherty St., Suite 105, Athens, GA 30601
- 70-74. N. Güven, Texas Tech University, Department of Geosciences, Lubbock, TX 79409-4109
75. R. E. Jackson, Roy F. Weston, Inc., 2301 Research Blvd., Rockville, MD 20850
76. K. S. Johnson, Earth Resource Associates, 1321 Greenbriar Drive, Norman, OK 73069
77. B. Y. Kanehiro, Berkeley Hydrotechnique, Inc., 2150 Shattuck Ave., Berkeley, CA 94704
78. J. Kasproicz, DOE-CHO, 9800 S. Cass Avenue, Chicago, IL 60439
- 79-83. C. R. Landis, Texas Tech University, Department of Geosciences, Lubbock, TX 79409-4109
84. R. Laughon, Battelle Memorial Institute, Office of Waste Technology Development, Battelle Project Management Division, 7000 S. Adams Street, Willowbrook, IL 60521
85. G. E. Likens, Director, The New York Botanical Garden, Institute of Ecosystem Studies, The Mary Flagler Cary Arboretum, Box AB, Millbrook, NY 12545
86. J. Long, Earth Sciences Division, Lawrence Berkeley Laboratory, One Cyclotron Road, Berkeley, CA 94720
87. C. J. Mankin, Director, Oklahoma Geological Survey, The University of Oklahoma, 830 Van Vleet Oval, Room 163, Norman, OK 73019
88. S. Mann, DOE-CHO, 9800 S. Cass Avenue, Chicago, IL 60439
89. W. C. McClain, Roy F. Weston, Inc., 2301 Research Blvd., Rockville, MD 20850
90. K. Mihm, DOE-Office of Civilian Radioactive Waste Management, 1000 Independence Ave., S.W., Washington, DC 20585
91. L. Myer, Earth Sciences Division, Lawrence Berkeley Laboratory, One Cyclotron Road, Berkeley, CA 94720
92. W. Newcomb, Battelle Memorial Institute, Office of Waste Technology Development, Battelle Project Management Division, 7000 S. Adams Street, Willowbrook, IL 60521
93. E. Patera, DOE-CHO, 9800 S. Cass Avenue, Chicago, IL 60439
94. T. Pigford, Department of Nuclear Engineering, College of Engineering, University of California, Berkeley, CA 94720
95. P. Potter, Department of Geology, University of Cincinnati, Cincinnati, OH 45221

96. E. Price, DOE-CHO, 9800 S. cass Avenue, Chicago, IL 60439
97. R. Robinson, Battelle Memorial Institute, Office of Waste Technology Development, Battelle Project Management Division, 7000 S. Adams Street, Willowbrook, IL 60521
98. R. Rothman, DOE-CHO, 9800 S. Cass Avenue, Chicago, IL 60439
99. J. E. Russell, Center for Tectonophysics, Texas A&M University, College Station, TX 77843
100. D. Siefken, Roy F. Weston, Inc., 2301 Research Blvd., Rockville, MD 20850
101. H. W. Smedes, DOE-CHO, 9800 S. Cass Avenue, Chicago, IL 60439
102. R. Stein, DOE-Office of Civilian Radioactive Waste Management, 1000 Independence Ave., S.W., Washington, DC 20585
103. G. Stirewalt, Battelle Memorial Institute, Office of Waste Technology Development, Battelle Project Management Division, 7000 S. Adams Street, Willowbrook, IL 60521
104. Ming-Chan Tu, Central Geological Survey, Box 968, Taipei, Taiwan, Republic of China
105. R. Wallace, DOE-Office of Civilian Radioactive Waste Management, 1000 Independence Ave., S.W., Washington, DC 20585
106. P. A. Witherspoon, Earth Sciences Division, Lawrence Berkeley Laboratory, One Cyclotron Road, Berkeley, CA 94720
107. F. J. Wobber, Ecological Research Division, Office of Health and Environmental Research, Office of Energy Research, MS-201, Department of Energy, Washington, DC 20545
108. W. Wowak, Roy F. Weston, Inc., 2301 Research Blvd., Rockville, MD 20850
109. A. Yonk, Battelle Memorial Institute, Office of Waste Technology Development, Battelle Project Management Division, 7000 S. Adams Street, Willowbrook, IL 60521
110. Office of Assistant Manager for Energy Research and Development, Oak Ridge Operations, P. O. Box 2001, U.S. Department of Energy, Oak Ridge, TN 37830
- 111-120. Office of Scientific and Technical Information, P. O. Box 62, Oak Ridge, TN 37831

